with those given ≥10 mg/kg/day of the mean ribavirin dose in this study [26.9% (49/182) *vs* 12.4% (26/209), $P < 0.001$] (data not shown). It seems possible to start ribavirin at a lower dose and increase it by degrees with monitoring of Hb level during treatment of patients with mild anaemia or ischemic heart disease, because the ribavirin dose appears to affect the viral relapse as the total dose over 48 weeks, not during the first 12 weeks.

In conclusion, our results have demonstrated that Peg-IFN α-2b is dose-dependently correlated with c-EVR and maintaining as high a drug dose of Peg-IFN α-2b as possible (≥1.2 μg/kg/week) during the first 12 weeks can yield higher c-EVR rates, leading to better treatment outcomes for patients with CH-C genotype 1.

ACKNOWLEDGMENTS AND DISCLOSURES

Other institutions and participants in the Osaka Liver Forum are: K Katayama, Osaka Koseinenkin Hospital; H Fukui, Yao Municipal Hospital; Y Doi, Otemae Hospital; A Kaneko, NTT West Osaka Hospital; T Kashihara, Itami City Hospital; K Kiriyama, Ashiya Municipal Hospital; T Nagase, Suita Municipal Hospital; M Inada, Toyonaka Municipal Hospital; K Fujimoto, National Hospital Organization Minami Wakayama Medical Center; K Suzuki, Saiseikai Senri Hospital; H Ogawa, Nishinomiya Municipal Central Hospital; S Kubota, Kano General Hospital; M Nishiuchi, Saso Hospital; and N Imaizumi, Osaka Kaisei Hospital.

This work was supported by a Grant-in-Aid for Research on Hepatitis and BSE from Ministry of Health Labour and Welfare of Japan, and Scientific Research from the Ministry of Education, Science, and Culture of Japan.

REFERENCES

1 Hayashi N, Takehara T. Antiviral therapy for chronic hepatitis C: past, present, and future. *J Gastroenterol* 2006; 41: 17–27.
2 Manns MP, McHutchison JG, Gordon SC *et al.* Peginterferon alfa-2b plus ribavirin compared with interferon alfa-2b plus ribavirin for initial treatment of chronic hepatitis C: a randomised trial. *Lancet* 2001; 358: 958–965.
3 Fried MW, Shiffman ML, Reddy KR *et al.* Peginterferon alfa-2a plus ribavirin for chronic hepatitis C virus infection. *N Engl J Med* 2002; 347: 975–982.
4 Hadziyannis SJ, Sette H Jr, Morgan TR *et al.* Peginterferon-alpha2a and ribavirin combination therapy in chronic hepatitis C: a randomized study of treatment duration and ribavirin dose. *Ann Intern Med* 2004; 140: 346–355.
5 Zeuzem S, Hultcrantz R, Bourliere M *et al.* Peginterferon alfa-2b plus ribavirin for treatment of chronic hepatitis C in previously untreated patients infected with HCV genotypes 2 or 3. *J Hepatol* 2004; 40: 993–999.
6 Hiramatsu N, Hayashi N, Kasahara A *et al.* Improvement of liver fibrosis in chronic hepatitis C patients treated with natural interferon alpha. *J Hepatol* 1995; 22: 135–142.
7 Kasahara A, Hayashi N, Mochizuki K *et al.* Risk factors for hepatocellular carcinoma and its incidence after interferon treatment in patients with chronic hepatitis C. Osaka Liver Disease Study Group. *Hepatology* 1998; 27: 1394–1402.
8 Ikeda K, Saitoh S, Arase Y *et al.* Effect of interferon therapy on hepatocellular carcinogenesis in patients with chronic hepatitis type C: a long-term observation study of 1,643 patients using statistical bias correction with proportional hazard analysis. *Hepatology* 1999; 29: 1124–1130.
9 Kasahara A, Tanaka H, Okanoue T *et al.* Interferon treatment improves survival in chronic hepatitis C patients showing biochemical as well as virological responses by preventing liver-related death. *J Viral Hepatitis* 2004; 11: 148–156.
10 Imai Y, Kasahara A, Tanaka H *et al.* Interferon therapy for aged patients with chronic hepatitis C: improved survival in patients exhibiting a biochemical response. *J Gastroenterol* 2004; 39: 1069–1077.
11 Davis GL, Wong JB, McHutchison JG, Manns MP, Harvey J, Albrecht J. Early virologic response to treatment with peginterferon alfa-2b plus ribavirin in patients with chronic hepatitis C. *Hepatology* 2003; 38: 645–652.
12 McHutchison JG, Manns M, Patel K *et al.* Adherence to combination therapy enhances sustained response in genotype-1-infected patients with chronic hepatitis C. *Gastroenterology* 2002; 123: 1061–1069.
13 Shiffman ML, Ghany MG, Morgan TR *et al.* Impact of reducing peginterferon alfa-2a and ribavirin dose during retreatment in patients with chronic hepatitis C. *Gastroenterology* 2007; 132: 103–112.
14 Reddy KR, Shiffman ML, Morgan TR *et al.* Impact of ribavirin dose reductions in hepatitis C virus genotype 1 patients completing peginterferon alfa-2a/ribavirin treatment. *Clin Gastroenterol Hepatol* 2007; 5: 124–129.
15 Shiffman ML, Salvatore J, Hubbard S *et al.* Treatment of chronic hepatitis C virus genotype 1 with peginterferon, ribavirin, and epoetin alpha. *Hepatology* 2007; 46: 371–379.
16 Paterson DL, Swindells S, Mohr J *et al.* Adherence to protease inhibitor therapy and outcomes in patients with HIV infection. *Ann Intern Med* 2000; 133: 21–30.
17 Strader DB, Wright T, Thomas DL, Seeff LB. Diagnosis, management, and treatment of hepatitis C. *Hepatology* 2004; 39: 1147–1171.
18 Dienstag JL, McHutchison JG. American Gastroenterological Association medical position statement on the management of hepatitis C. *Gastroenterology* 2006; 130: 225–230.
19 Poynard T, Marcellin P, Lee SS *et al.* Randomised trial of interferon alpha2b plus ribavirin for 48 weeks or for 24 weeks versus interferon alpha2b plus placebo for 48 weeks for treatment of chronic infection with hepatitis C virus. International Hepatitis Interventional Therapy Group (IHIT). *Lancet* 1998; 352: 1426–1432.
20 McHutchison JG, Gordon SC, Schiff ER *et al.* Interferon alfa-2b alone or in combination with ribavirin as initial treatment for chronic hepatitis C. Hepatitis Interventional Therapy Group. *N Engl J Med* 1998; 339: 1485–1492.
21 Davis GL, Esteban-Mur R, Rustgi V *et al.* Interferon alfa-2b alone or in combination with ribavirin for the treatment of relapse of chronic hepatitis C. International Hepatitis Interventional Therapy Group. *N Engl J Med* 1998; 339: 1493–1499.

© 2009 The Authors
Journal compilation © 2009 Blackwell Publishing Ltd

22 Hiramatsu N, Kasahara A, Nakanishi F *et al.* The significance of interferon and ribavirin combination therapy followed by interferon monotherapy for patients with chronic hepatitis C in Japan. *Hepatol Res* 2004; 29: 142–147.
23 Bronowicki JP, Ouzan D, Asselah T *et al.* Effect of ribavirin in genotype 1 patients with hepatitis C responding to pegylated interferon alfa-2a plus ribavirin. *Gastroenterology* 2006; 131: 1040–1048.
24 Hiramatsu N, Oze T, Yakushijin T, *et al.* Ribavirin dose reduction raises relapse rate dose-dependently in genotype 1 patients with hepatitis C responding to pegylated interferon alfa-2b plus ribavirin. *J Viral Hepat* 2009; In press.

© 2009 The Authors
Journal compilation © 2009 Blackwell Publishing Ltd

LGP2 is a positive regulator of RIG-I– and MDA5-mediated antiviral responses

Takashi Satoh[a,1], Hiroki Kato[a,1,2], Yutaro Kumagai[a], Mitsutoshi Yoneyama[b,c], Shintaro Sato[a,3], Kazufumi Matsushita[a], Tohru Tsujimura[d], Takashi Fujita[b], Shizuo Akira[a,4], and Osamu Takeuchi[a]

[a]Laboratory of Host Defense, WPI Immunology Frontier Research Center, Research Institute for Microbial Diseases, Osaka University, Osaka 565-0871, Japan; [b]Department of Genetics and Molecular Biology, Institute for Virus Research, and Laboratory of Molecular Cell Biology, Graduate School of Biostudies, Kyoto University, Kyoto 606-8507, Japan; [c]PRESTO, Japan Science and Technology Agency, Saitama, Japan; and [d]Department of Pathology, Hyogo College of Medicine, Hyogo 663-8501, Japan

Contributed by Shizuo Akira, November 10, 2009 (sent for review October 30, 2009)

RNA virus infection is recognized by retinoic acid-inducible gene (RIG)-I–like receptors (RLRs), RIG-I, and melanoma differentiation–associated gene 5 (MDA5) in the cytoplasm. RLRs are comprised of N-terminal caspase-recruitment domains (CARDs) and a DExD/H-box helicase domain. The third member of the RLR family, LGP2, lacks any CARDs and was originally identified as a negative regulator of RLR signaling. In the present study, we generated mice lacking LGP2 and found that LGP2 was required for RIG-I– and MDA5-mediated antiviral responses. In particular, LGP2 was essential for type I IFN production in response to picornaviridae infection. Overexpression of the CARDs from RIG-I and MDA5 in *Lgp2*$^{-/-}$ fibroblasts activated the IFN-β promoter, suggesting that LGP2 acts upstream of RIG-I and MDA5. We further examined the role of the LGP2 helicase domain by generating mice harboring a point mutation of Lys-30 to Ala (*Lgp2*$^{K30A/K30A}$) that abrogated the LGP2 ATPase activity. *Lgp2*$^{K30A/K30A}$ dendritic cells showed impaired IFN-β productions in response to various RNA viruses to extents similar to those of *Lgp2*$^{-/-}$ cells. *Lgp2*$^{-/-}$ and *Lgp2*$^{K30A/K30A}$ mice were highly susceptible to encephalomyocarditis virus infection. Nevertheless, LGP2 and its ATPase activity were dispensable for the responses to synthetic RNA ligands for MDA5 and RIG-I. Taken together, the present data suggest that LGP2 facilitates viral RNA recognition by RIG-I and MDA5 through its ATPase domain.

innate immunity | type I interferon | virus infection

RNA virus infection is initially recognized by host pattern recognition receptors, including retinoic acid-inducible gene (RIG)-I–like receptors (RLRs) and Toll-like receptors (TLRs), which induce antiviral responses such as the productions of type I IFNs and proinflammatory cytokines (1–4). The RLR family comprises RIG-I, melanoma differentiation-associated gene 5 (MDA5) and LGP2. RLRs harbor a central DExD/H-box helicase domain and a C-terminal regulatory domain (RD). RIG-I and MDA5 also contain two N-terminal caspase recruitment domains (CARDs), whereas LGP2 does not. RIG-I recognizes relatively short double-stranded (ds) RNAs (up to 1 kb), and the presence of a 5′ triphosphate end greatly potentiates its type I IFN-inducing activity (5–7). On the other hand, MDA5 detects long dsRNAs (more than 2 kb), such as polyinosinic polycytidylic acid (poly I:C). Analyses of *Rig-I*–deficient (*Rig-I*$^{-/-}$) and *Mda5*$^{-/-}$ mice have shown that RIG-I is essential for the production of type I IFNs in response to various RNA viruses, including vesicular stomatitis virus (VSV), Sendai virus (SeV), Japanese encephalitis virus (JEV), and influenza virus, whereas MDA5 is critical for the detection of picornaviridae such as encephalomyocarditis virus (EMCV) and mengovirus (8, 9). Some RNA viruses such as West Nile virus and reovirus are recognized by both RIG-I and MDA5 (10, 11). RIG-I is also reported to be involved in the recognition of foreign DNA in the cytoplasm through transcription of the DNA to dsRNA by polymerase III (12, 13).

The C-terminal RDs of RLRs are responsible for binding to dsRNAs (3). However, the functions of the helicase domains of the RLR family members have not yet been clarified. Although the RIG-I helicase domain has the ability to unwind dsRNA, this activity is not correlated with the level of IFN production (14). A recent report proposed that the RIG-I ATPase activity is required for translocation of RIG-I on dsRNA (15). The N-terminal CARDs of RIG-I and MDA5 trigger intracellular signaling pathways via IFN-β promoter stimulator (IPS)–1 (also known as MAVS, VISA, or CARDIF), an adaptor molecule possessing an N-terminal CARD (16). IPS-1 subsequently activates two IκB kinase (IKK)–related kinases, IKK-*i*, and TANK-binding kinase 1 (TBK1). These kinases phosphorylate IFN-regulatory factor (IRF) 3 and IRF7, which activate the transcription of genes encoding type I IFNs and IFN-inducible genes. The produced type I IFNs alert the surrounding cells by triggering signaling cascades that lead to phosphorylation and nuclear translocation of STAT1 (1, 2).

The third RLR family member LGP2, also known as Dhx58, harbors a DExD/H-box helicase domain and a C-terminal RD but lacks any CARDs (17). In vitro studies have suggested that LGP2 negatively regulates RIG-I–mediated dsRNA recognition (18). Several models have been proposed for the mechanisms of this inhibition. The first model is that LGP2 binds to viral dsRNA and prevents RIG-I– and MDA5-mediated recognition (18). The second model is that LGP2 inhibits multimerization of RIG-I and its interaction with IPS-1 via the RD of LGP2 (19). The third model is that LGP2 competes with IKK-*i* for recruitment to IPS-1, thereby suppressing RLR signaling (20). Structural analyses of the C-terminal domain of LGP2 have revealed that LGP2 can bind to the termini of dsRNAs more firmly than MDA5 (21–23). A previous report showed that *Lgp2*$^{-/-}$mice exhibit enhanced production of type I IFNs in response to poly I:C stimulation and VSV infection, whereas the response to EMCV is suppressed (24). Therefore, the role of LGP2 in the negative or positive regulation of RLR signaling has not yet been fully clarified.

In the present study, we generated *Lgp2*$^{-/-}$ mice and mice harboring a point mutation in the LGP2 helicase domain (K30A), and examined their responses to RNA viruses recognized by RIG-I and MDA5. Conventional dendritic cells (cDCs) and mouse embryonic fibroblasts (MEFs) obtained from *Lgp2*$^{-/-}$ mice showed severely impaired IFN responses to infections with picornaviruses, which are recognized by MDA5. Furthermore,

Author contributions: T.S., H.K., S.A., and O.T. designed research; T.S., H.K., Y.K., S.S., K.M., and T.T. performed research; M.Y. and T.F. contributed new reagents/analytic tools; T.S., H.K., T.T., S.A., and O.T. analyzed data; and S.A. and O.T. wrote the paper.

The authors declare no conflict of interest.

See Commentary on page 1261.

[1]T.S. and H.K. contributed equally to this work.

[2]Present address: Program in Molecular Medicine, University of Massachusetts, Worcester, MA 01605.

[3]Present address: Division of Mucosal Immunology, Department of Microbiology and Immunology, Institute of Medical Science, University of Tokyo, Tokyo 108-8639, Japan.

[4]To whom correspondence should be addressed. E-mail: sakira@biken.osaka-u.ac.jp.

This article contains supporting information online at www.pnas.org/cgi/content/full/0912986107/DCSupplemental.

the responses to viruses recognized by RIG-I were also impaired in $Lgp2^{-/-}$ cells. In contrast, the IFN productions in response to synthetic RNAs, poly I:C and RNA synthesized by T7 polymerase, were comparable between wild-type (WT) and $Lgp2^{-/-}$ or $Lgp2^{K30A/K30A}$ cells. $Lgp2^{-/-}$ and $Lgp2^{K30A/K30A}$ mice were highly susceptible to infection with EMCV. Taken together, the present results demonstrate that LGP2 acts as a positive, but not negative, regulator of RIG-I– and MDA5-mediated viral recognition.

Results

Generation of Mice Lacking Lgp2. To investigate the physiological role of LGP2 in vivo, we established $Lgp2^{-/-}$ mice (Fig. S1 *A* and *B*). As reported previously, the expression of *Lgp2* mRNA was highly induced in response to IFN-β stimulation in MEFs (Fig. S1*C*) (17). Expression of *Lgp2* mRNA was not detected in $Lgp2^{-/-}$ MEFs, whereas the expression levels of *Rig-I* and *Mda5* mRNAs were comparable between WT and $Lgp2^{-/-}$ cells (Fig. S1*C*). The $Lgp2^{-/-}$ progenies obtained from $Lgp2^{+/-}$ intercrosses were lower than the expected Mendelian ratio (Fig. S2*A*), indicating that homozygous mutations of the *Lgp2* gene cause embryonic lethality at a high frequency. In addition, adult female $Lgp2^{-/-}$ mice showed an enlarged uterus filled with fluid resulting from vaginal atresia (Fig. S2 *B* and *C*).

Role of LGP2 in Type I IFN and Cytokine Productions in Response to RNA Viruses. First, we examined the production of IFN-β in cDCs derived from bone marrow (BM) in the presence of GM-CSF after infection with a variety of RNA viruses (Fig. 1). The productions of IFN-β in response to picornaviridae, EMCV, and mengovirus were severely impaired in $Lgp2^{-/-}$ cDCs compared with WT cells (Fig. 1*A*). IL-6 production induced by EMCV infection was also severely impaired in $Lgp2^{-/-}$ cells (Fig. 1*B*). Furthermore, LGP2 was involved in the productions of IFN-β in response to several RNA viruses recognized by RIG-I, such as VSV, SeV, and JEV (Fig. 1*A*). IFN-β production in response to reovirus, a dsRNA virus, was also impaired in $Lgp2^{-/-}$ cells (Fig. 1*A*). In contrast, the IFN-β productions in response to infection with influenza virus were comparable between WT and $Lgp2^{-/-}$ cDCs (Fig. 1*A*). Stimulation with CpG-DNA, a TLR9 ligand, induced comparable amounts of IFN-β in WT and $Lgp2^{-/-}$ cells (Fig. 1*A*).

Next, we examined whether the defect in type I IFN production in response to EMCV was controlled at the mRNA level. The expressions of the genes encoding IFN-β, CXCL10 and IL-6 after infection with EMCV were severely impaired in $Lgp2^{-/-}$ macrophages (Fig. 2*A*). However, the influenza virus-induced expressions of IFN-β and CXCL10 mRNAs were comparable between WT and $Lgp2^{-/-}$ MEFs throughout the whole time course (Fig. 2*B*). Therefore, it is unlikely that LGP2 negatively regulates RIG-I–mediated responses, even during the later period of infection. These results indicate that LGP2 is involved in positive, but not negative, regulation of virus recognition by MDA5 and RIG-I, with the exception of influenza virus.

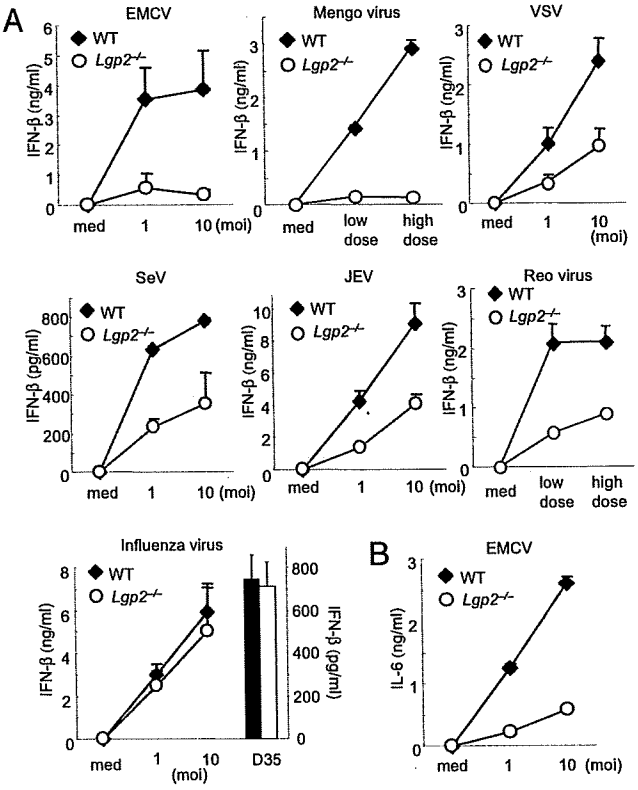

Fig. 1. Role of LGP2 in type I IFN production in response to various RNA viruses. (*A* and *B*) BM-derived cDCs from WT and $Lgp2^{-/-}$ mice were exposed to the indicated viruses or treated with 1 μM CpG-DNA (D35) for 24 h. The concentrations of IFN-β (*A*) and IL-6 (*B*) in the culture supernatants were measured by ELISA. moi, multiplicity of infection; med, medium alone. Data are shown as means ± SD and are representative of at least three independent experiments.

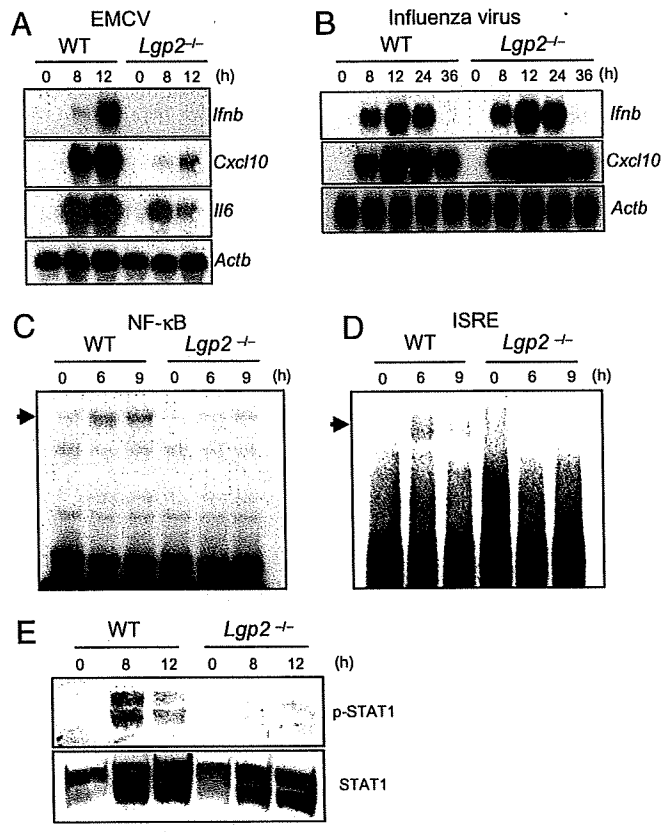

Fig. 2. Role of LGP2 in the activation of signaling pathways leading to IFN-inducible gene expression. (*A*) Total RNAs extracted from WT and $Lgp2^{-/-}$ macrophages infected with EMCV were subjected to Northern blot analyses for the expressions of *Ifnb*, *Cxcl10*, *Il6*, and *Actb* mRNAs. (*B*) WT and $Lgp2^{-/-}$ MEFs were infected with influenza virus followed by isolation of the total RNA. The expressions of *Ifnb*, *Cxcl10*, and *Actb* mRNAs were determined by Northern blot analyses. (*C* and *D*) Nuclear extracts were prepared from WT and $Lgp2^{-/-}$ macrophages infected with EMCV for the indicated periods. The binding activities of DNA to NF-κB (C) and ISREs (*D*) were determined by EMSAs. (*E*) Cell lysates were prepared from WT and $Lgp2^{-/-}$ macrophages infected with EMCV and probed with anti–phospho-STAT-1 and anti-STAT1 antibodies. The data are representative of at least three independent experiments.

Cell Type-Specific Involvement of LGP2 in EMCV Recognition. We previously showed that RIG-I– and MDA5-dependent RNA virus recognition occurs in cDCs but not in plasmacytoid dendritic cells (pDCs) (8). To determine whether LGP2 functions in a cell type–specific fashion, $B220^{-}CD11c^{+}$ cDCs and $CD11c^{+}B220^{+}$ pDCs were purified from WT and $Lgp2^{-/-}$ splenocytes. EMCV-induced IFN-β production was severely impaired in $Lgp2^{-/-}$ splenic cDCs compared with WT cDCs, whereas splenic pDCs from WT and $Lgp2^{-/-}$ mice produced comparable amounts of IFN-β (Fig. S3). These data indicate that LGP2 functions in cDCs but not in pDCs.

LGP2 Is Essential for Triggering RLR Signaling Pathways. To investigate whether LGP2 regulates the primary responses to RNA virus infections, we examined the activation of intracellular signaling pathways. Electrophoretic mobility shift assays (EMSAs) revealed that the activations of NF-κB and IFN-stimulated regulatory elements (ISREs) in response to EMCV infection were severely impaired in $Lgp2^{-/-}$ cells (Fig. 2 *C* and *D*). Furthermore, the phosphorylation of STAT1 was abrogated in $Lgp2^{-/-}$ cells (Fig. 2*E*). Nevertheless, the expressions of *Lgp2* in response to IFN-β treatment were not altered in $Rig\text{-}I^{-/-}$ and $Mda5^{-/-}$ cells (Fig. S4). These results suggest that LGP2 is required for the initial recognition of EMCV, leading to activation of transcription factors involved in the expression of type I IFNs.

Next, we examined whether the expression of *Lgp2* could rescue the virus-mediated IFN responses. IFN-β–dependent reporter gene expression was induced in response to EMCV infection in WT, but not in $Lgp2^{-/-}$, MEFs (Fig. 3*A*). Expression of exogenous LGP2 in $Lgp2^{-/-}$ cells restored the EMCV-induced IFN-β promoter activity as well as IFN-β production (Fig. 3 *A* and *B*). Although overexpression of either LGP2 or MDA5 alone in $Lgp2^{-/-}Mda5^{-/-}$ MEFs failed to confer EMCV-induced IFN-β promoter activity, coexpression of both LGP2 and MDA5 restored EMCV responsiveness (Fig. 3*C*). Overexpression of the CARDs from RIG-I or MDA5 in $Lgp2^{-/-}$ MEFs activated the IFN-β promoter (Fig. 3*D*), suggesting that LGP2 functions upstream of RIG-I and MDA5.

Normal IFN Responses of $LGP2^{-/-}$ cells to Exogenously Transfected RNAs. We examined the responses of $Lgp2^{-/-}$ cells to synthetic RNAs recognized by RIG-I and MDA5. Unexpectedly, WT and $Lgp2^{-/-}$ cDCs produced comparable amounts of IFN-β in response to poly I:C, in vitro–transcribed dsRNA and RNA with a 5′ triphosphate end (Tri-P) (Fig. 4*A*). Similarly, Lgp2-deficiency did not affect the IFN-β productions in response to the synthesized RNAs in fibroblasts (Fig. 4*A*). In addition, no differences were observed in the responses to the various concentrations of poly I:C examined (Fig. 4*B*). These data suggest that LGP2 is dispensable for the recognition of synthesized dsRNA and 5′ triphosphate RNA.

Function of LGP2 ATPase Domain in Type I IFN Responses to Virus Infections. The recognition of dsRNA and RNA viruses by RIG-I or MDA5 requires ATPase activity (17, 25). To examine the role of the LGP2 ATPase activity in LGP2-mediated virus recognition, we reconstituted $Lgp2^{-/-}$ MEFs with WT LGP2 or LGP2-K30A harboring a Lys-to-Ala point mutation in the Walker ATP-binding motif using a retrovirus system. Expression of WT LGP2 in $Lgp2^{-/-}$ MEFs conferred IFN-β promoter activity as well as IFN-β production in response to EMCV, whereas expression of LGP2-K30A failed to confer these responses to EMCV infection (Fig. 5 *A* and *B*).

To further examine the role of the LGP2 ATPase activity in vivo, we generated mice harboring the LGP2 K30A point mutation (Fig. S5 *A* and *B*). Expression of *Lgp2* mRNA was comparably induced in response to IFN-β stimulation in WT and $Lgp2^{K30A/K30A}$ MEFs (Fig. S5*C*). We confirmed the insertion of

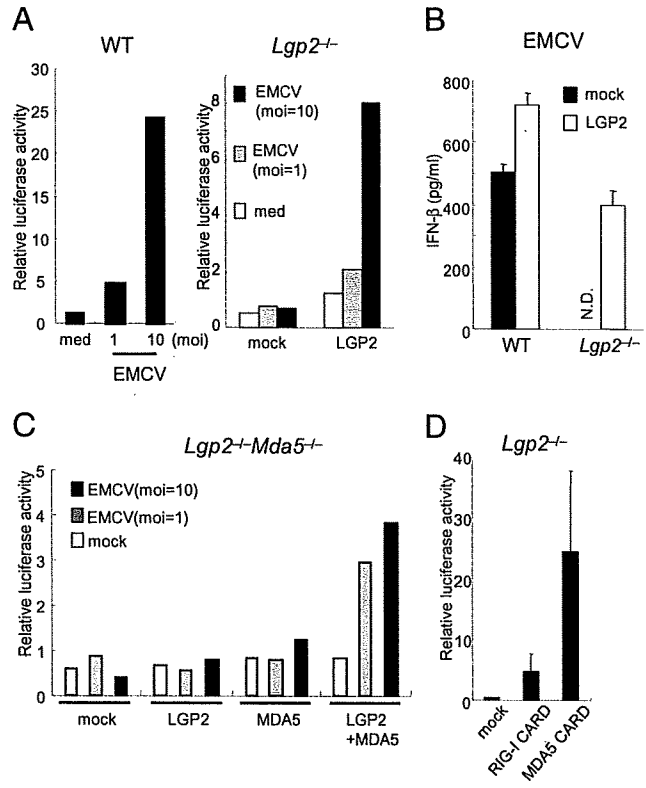

Fig. 3. LGP2 acts in the upstream of RIG-I and MDA5. (*A*) WT and $Lgp2^{-/-}$ MEFs were transiently transfected with the IFN-β promoter construct together with expression plasmids encoding LGP2. The cells were infected with EMCV for 8 h and then lysed. The cell lysates were analyzed by a luciferase assay. (*B*) WT and $Lgp2^{-/-}$ MEFs were infected with a retrovirus expressing *Lgp2*. At 2 days after infection, the cells were exposed to EMCV for 24 h. The IFN-β concentrations in the culture supernatants were measured by ELISA. N.D., not detected. (*C*) $Lgp2^{-/-}Mda5^{-/-}$ MEFs were transiently transfected with the IFN-β promoter reporter construct together with the indicated expression plasmids. After 24 h, the cells were infected with EMCV for 8 h and then lysed. The cell lysates were analyzed by a luciferase assay. (*D*) $Lgp2^{-/-}$ MEFs were transiently transfected with the IFN-β promoter construct together with expression plasmids encoding the CARDs of RIG-I or MDA5 and then lysed at 48 h after transfection. The cell lysates were analyzed by a luciferase assay.

the point mutation by sequencing analysis (Fig. S5*D*). The $Lgp2^{K30A/K30A}$ mice were born at the expected Mendelian ratio, and did not show any developmental defects. We examined the IFN-β productions in cDCs in response to infections with RNA viruses. The IFN-β productions in response to infections with EMCV, mengovirus, VSV, SeV, and reovirus, but not with influenza virus, were severely impaired in $Lgp2^{K30A/K30A}$ cDCs compared with WT cells (Fig. 5*C*). The IL-6 production in response to EMCV infection was also impaired in $Lgp2^{K30A/K30A}$ cDCs (Fig. 5*D*). The defects observed in $Lgp2^{K30A/K30A}$ cDCs were as severe as those observed in $Lgp2^{-/-}$ cDCs, suggesting that the ATPase activity of LGP2 is essential for the recognition of viruses. The productions of IFN-β in response to transfections of synthetic RNAs and poly I:C were comparable between WT and $Lgp2^{K30A/K30A}$ cells (Fig. 5*E*), further confirming that LGP2 is not involved in the responses to the transfection of synthetic RNAs. Taken together, these results indicate that the ATPase activity of LGP2 is essential for LGP2 to function as a positive regulator in MEFs. This finding is in marked contrast to in vitro experiments in which overexpression of WT LGP2 and LGP2-K30A in HEK293 cells suppressed RIG-I–mediated IFN-β promoter activity (Fig. S6), suggesting that overexpression of

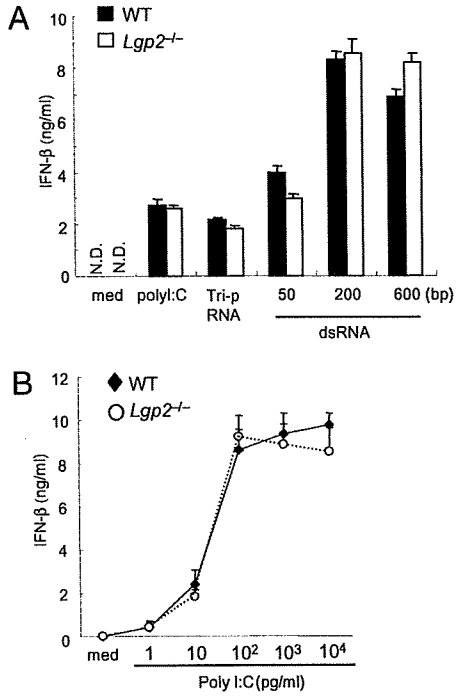

Fig. 4. Role of LGP2 in the recognition of exogenously transfected RNAs. (*A*) WT and *Lgp2*$^{-/-}$ MEFs were stimulated with triphosphate RNA, in vitro–transcribed dsRNA (1 μg/mL) or poly I:C complexed with Lipofectamine 2000 for 24 h. The IFN-β concentrations in the culture supernatants were measured by ELISA. med, medium; N.D., not detected. Data are shown as the means ± SD of triplicate samples. Similar results were obtained in three independent experiments. (*B*) WT and *Lgp2*$^{-/-}$ MEFs were transfected with the indicated amounts of poly I:C complexed with Lipofectamine 2000. The IFN-β concentrations in the culture supernatants were measured by ELISA.

LGP2 in HEK293 cells nonspecifically inhibits the RIG-I–mediated pathway.

Role of LGP2 and Its ATPase Activity in Antiviral Host Defenses In Vivo. Finally, we assessed the role of LGP2 and its ATPase activity in antiviral responses in vivo. When *Lgp2*$^{-/-}$ mice were challenged with EMCV, IFN-β production was not detected in their sera (Fig. 6*A*). Furthermore, *Lgp2*$^{-/-}$ mice were highly susceptible to EMCV infection compared with their littermate controls (Fig. 6*C*). Consistent with the increased susceptibility to EMCV, the viral titer in the heart was remarkably higher in *Lgp2*$^{-/-}$ mice than in control mice (Fig. 6*E*). Similar to the results for *Lgp2*$^{-/-}$ mice, *Lgp2*$^{K30A/K30A}$ mice showed severe defects in IFN-β production in response to EMCV infection (Fig. 6*B*). *Lgp2*$^{K30A/K30A}$ mice were highly susceptible to infection with EMCV, with highly increased viral titers in their hearts (Fig. 6 *D* and *F*). These data indicate that LGP2 also plays a key role in the host defenses against RNA viruses recognized by MDA5 in vivo.

Discussion

The present data clearly demonstrate that LGP2 acts as a positive regulator of MDA5- and RIG-I–mediated viral recognition, except for influenza virus. These findings are in contrast to the conclusions deduced from previous in vitro studies and a report on Lgp2 knockout mice generated by another group (17, 18, 20, 24). LGP2 is particularly important for the recognition of picornaviruses, including EMCV and mengovirus, among RNA viruses. Analyses of the activation status of signaling molecules revealed that LGP2 was involved in the primary recognition of EMCV upstream of MDA5. LGP2 was also involved in the recognition of RNA viruses recognized by RIG-I, such as VSV

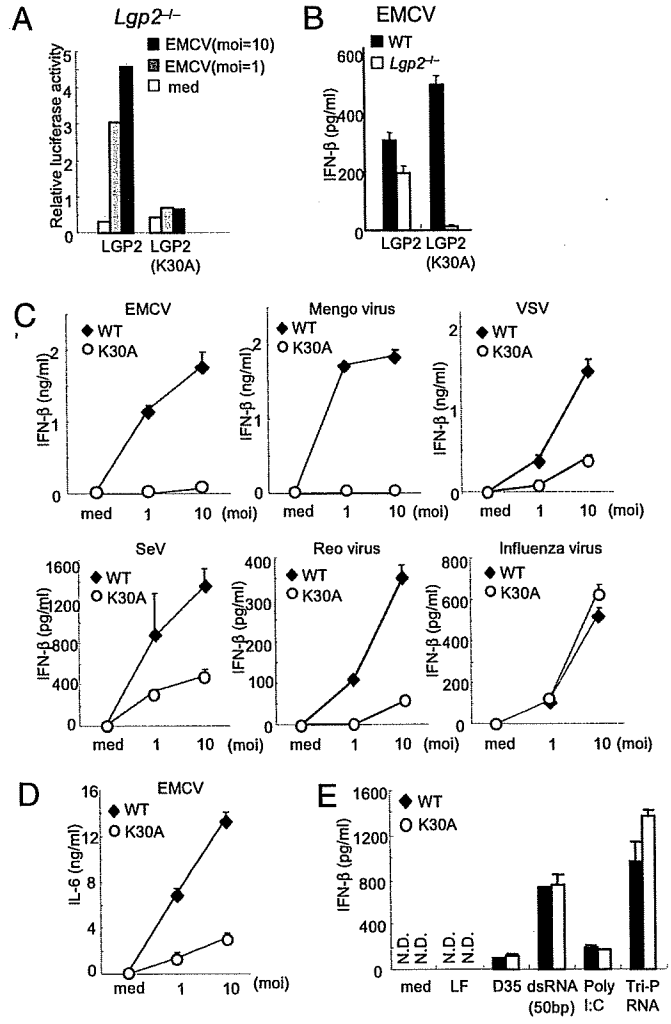

Fig. 5. Essential role of the LGP2 ATPase activity in the recognition of RNA viruses. (*A*) *Lgp2*$^{-/-}$ MEFs were transiently transfected with the IFN-β promoter construct together with expression plasmids encoding *LGP2 or LGP2* (K30A). The cells were infected with EMCV for 8 h and then lysed. The cell lysates were analyzed by a luciferase assay. (*B*) WT and *Lgp2*$^{-/-}$ MEFs were infected with retroviruses expressing *LGP2 or LGP2 (K30A)*. At 2 days after infection, the cells were exposed to EMCV for 24 h and the IFN-β concentrations in the culture supernatants were measured by ELISA. (*C* and *D*) WT and *Lgp2*$^{K30A/K30A}$ (K30A) mice were exposed to the indicated RNA viruses for 24 h. The concentrations of IFN-β (*C*) and IL-6 (*D*) in the culture supernatants were measured by ELISA. (*E*) WT and *Lgp2*$^{K30A/K30A}$ cDCs were transfected with the indicated RNAs for 24 h. The concentrations of IFN-β in the culture supernatants were measured by ELISA. moi, multiplicity of infection; med, medium alone; LF, lipofectamine alone. Data are shown as means ± SD and are representative of at least three independent experiments.

and SeV, although the defects in the responses to these viruses observed in *Lgp2*$^{-/-}$ cells were not as severe as the defects in the responses to picornaviruses. Surprisingly, *Lgp2*$^{-/-}$ cells responded efficiently to synthetic RNA compounds, including poly I:C, dsRNA transcribed in vitro using T7 polymerase and 5′ triphosphate RNA.

Cells from *Lgp2*$^{K30A/K30A}$ mice showed severe defects in the IFN responses to RNA viruses to extents similar to those of *Lgp2*$^{-/-}$ cells. Furthermore, expression of the LGP2-K30A mutant protein in *Lgp2*$^{-/-}$ cells failed to restore the EMCV responsiveness. These results clearly demonstrate that the ATPase domain of LGP2 is a prerequisite for its function in recognizing RNA virus infection. Recent advances in studies on DExD/H-box

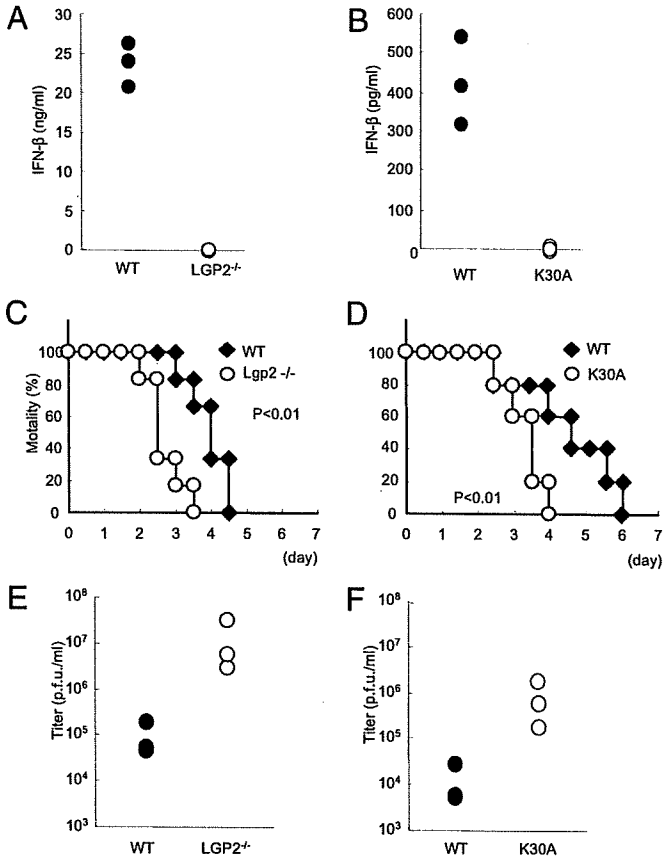

Fig. 6. Role of LGP2 in host defense against EMCV infection in vivo. (*A* and *B*) WT and littermate $Lgp2^{-/-}$ mice (*A*) or WT and littermate $Lgp2^{K30A/K30A}$ (K30A) mice (*B*) were i.v. inoculated with 1×10^7 pfu EMCV. Serum samples were obtained at 4 h after injection, and the IFN-β concentrations were determined by ELISA. (*C* and *D*) Survival rates of WT and $Lgp2^{-/-}$ mice (*C*) or WT and littermate $Lgp2^{K30A/K30A}$ mice (*D*) intraperitoneally infected with 1×10^2 pfu EMCV were monitored every 12 h for 5 days. (*E* and *F*) WT and littermate $Lgp2^{-/-}$mice (*E*) or WT and littermate $Lgp2^{K30A/K30A}$ mice (*F*) were infected i.p. with 1×10^2 pfu EMCV. After 48 h, the mice were killed and the virus titers in their hearts were determined by a plaque assay.

proteins have revealed that these proteins are involved in all aspects of RNA metabolism including translation initiation, mRNA splicing, and nuclear transport (26). Although DExD/H-box proteins, including RIG-I, are known to exhibit ATP-dependent RNA helicase activity in vitro, many DExD/H-box proteins have a more general RNA conformational change activity, rather than just a duplex-unwinding activity. In this regard, it is tempting to speculate that LGP2 functions to modify viral RNA by removing proteins from viral ribonucleoprotein (RNP) complexes or unwinding complex RNA structures to facilitate MDA5- and RIG-I–mediated recognition of dsRNA. Picornaviruses replicate in association with the cytoplasmic membranes of infected cells (27). It is therefore possible that LGP2 makes viral RNP complexes more accessible to MDA5 and RIG-I by changing their intracellular localization.

RLRs contain a C-terminal regulatory domain that is responsible for the binding to dsRNAs. The recent solution of the RLR C-terminal regulatory domain structures showed that the LGP2 and RIG-I C-terminal domains have a large basic surface, formed by the RNA-binding loop, and that the LGP2 C-terminal domain binds to the termini of dsRNAs (14, 21–23, 28). Although the MDA5 C-terminal domain also has a large basic surface, it is extensively flat because of the open conformation of the RNA-binding loop (21). Consequently, the RNA-binding activity of MDA5 is much weaker than those of RIG-I and LGP2. The present study has demonstrated that LGP2 is more profoundly required for the recognition of RNA viruses detected by MDA5 than for those detected by RIG-I. MDA5 may require LGP2 for efficient recruitment of viral dsRNAs to facilitate the initiation of signaling, and LGP2 appears to be more important for MDA5 than for RIG-I, possibly because of differences in their affinities for dsRNAs.

Although LGP2 is involved in the responses to various RNA viruses, influenza virus infection induced normal type I IFN production in $Lgp2^{-/-}$ cells. Type I IFN production in response to influenza virus was dependent on RIG-I but not on MDA5. We (5) and Pichlmair et al. (29) previously showed that phosphatase treatment of genomic RNA derived from influenza virus completely abolishes its type I IFN–inducing activity via RIG-I, indicating that a phosphate group at the 5′ end of the influenza virus genome is responsible for RIG-I–mediated recognition. Therefore, the 5′ triphosphate RNA present on viral genomes may be readily accessible to RIG-I without modification by LGP2.

Venkataraman et al. (24) reported that LGP2 acts as a negative regulator for the recognition of VSV and poly I:C, and a positive regulator for EMCV-induced IFN responses in macrophages by generating $Lgp2^{-/-}$ mice. Their results are contradictory to our present findings in terms of the responses to poly I:C and viruses recognized by RIG-I. Although we do not have a clear explanation for these discrepancies, expression of LGP2 in $Lgp2^{-/-}$ cells restored the responses to VSV and EMCV. Furthermore, we found that both $Lgp2^{-/-}$ and $Lgp2^{K30A/K30A}$ cells showed defects in IFN production in response to certain viruses recognized by RIG-I and showed normal responses to dsRNA specimens. Therefore, we believe that LGP2 acts as a positive, but not negative, regulator of RIG-I– and MDA5-dependent recognition of RNA virus infection and plays a pivotal role in antiviral responses in vivo.

Although some of the female $Lgp2^{-/-}$ mice showed a defect in the development of the vagina, $Lgp2^{K30A/K30A}$ mice did not exhibit any developmental abnormalities. Although the ATPase domain was essential for antiviral responses, the vaginal atresia was regulated by LGP2 independently of its ATPase activity. Given that $Rig\text{-}I^{-/-}$ mice showed fetal liver apoptosis at day 13, it will be interesting to analyze the role of the RIG-I ATPase activity in the control of development. Further studies are required to determine the roles of the RLR family members in controlling mammalian development.

Given that many RLR signaling molecules are inhibited by viral components, LGP2 may also be a target of the escape mechanisms exerted by various RNA viruses. Future studies aimed at identifying the mechanisms by which LGP2 modifies viral RNP complexes will help us to understand the roles of the innate immune system in intracellular virus recognition, and will lead to the development of new strategies to manipulate antiviral responses.

Materials and Methods

Generation of $Lgp2^{-/-}$ and $Lgp2^{K30A/K30A}$ Mice. The *Lgp2* gene was isolated from genomic DNA extracted from embryonic stem (ES) cells (GSI-I) by PCR. The targeting vector was constructed by replacing a 4-kb fragment encoding the *Lgp2* ORF (including the DExH/H box) with a neomycin-resistance gene cassette (*neo*), and inserting herpes simplex virus thymidine kinase (HSV-TK) driven by the PGK promoter into the genomic fragment for negative selection. After the targeting vector was transfected into ES cells, G418 and gancyclovir double-resistant colonies were selected and screened by PCR, and recombination was confirmed by Southern blotting. Homologous recombinants were microinjected into C57BL/6 female mice, and heterozygous F1 progenies were intercrossed to obtain $Lgp2^{-/-}$ mice. $Lgp2^{-/-}$ and littermate control mice were used for subsequent experiments.

A point mutation was inserted into a genomic fragment harboring the exon encoding Lys-30 of murine *Lgp2* by site-directed mutagenesis (Clontech) to replace this residue with Ala. A targeting vector was constructed with this genomic fragment and electroporated into ES cells. Homologous recombinants were selected and microinjected into C57BL/6 female mice,

and heterozygous F1 progenies were crossed with CAG-Cre transgenic mice to excise the *neo* cassette. Next, the CAG-Cre transgene was removed from $Lgp2^{+/K30A}$ mice by crossing the mice with C57BL/6 mice. $Lgp2^{K30A/K30A}$ and littermate control mice were used for subsequent experiments.

All animal experiments were carried out with the approval of the Animal Research Committee of the Research Institute for Microbial Diseases (Osaka University).

Mice, Cells, and Reagents. $Rig\text{-}I^{-/-}$ and $Lgp2^{-/-}Mda5^{-/-}$ MEFs were prepared from embryos on 129Sv and C57BL/6 backgrounds derived at 11.5 days post coitum. BM-derived DCs were generated in RPMI medium 1640 containing 10% FCS, 50 mM 2-mercaptoethanol, and 10 ng/mL GM-CSF (PeproTech). pDCs and cDCs were isolated from the spleen by MACS using anti-B220 and anti-CD11c microbeads (Miltenyi Biotech). Poly I:C was purchased from Amersham Biosciences. RNAs were complexed with the cationic lipid Lipofectamine 2000 (Invitrogen) and added to cells. A/D-type CpG-oligodeoxynucleotides (D35) were synthesized by Hokkaido System Science. In vitro–transcribed dsRNA and triphosphate RNA were described previously (5, 9). Antibodies against phospho-STAT1 and STAT1 (Cell Signaling) were used for Western blotting as described previously (8).

Viruses. VSV, VSV lacking an M protein variant (NCP), influenza virus ΔNS1, JEV, EMCV, and mengovirus were described previously (9). SeV lacking V protein (V–) was kindly provided by Dr. A. Kato. Reovirus was kindly provided by Dr. T. Dermody.

Northern Blotting. Total RNA was extracted from peritoneal macrophages infected with EMCV or MEFs infected with influenza virus using TRIzol reagent (Invitrogen). The obtained RNA was electrophoresed, transferred to nylon membranes, and hybridized with various cDNA probes. To detect the expression of *Lgp2* mRNA, a 326-bp fragment (772–1098) was used as a probe.

EMSA. Peritoneal macrophages (3×10^6) were infected with EMCV for various periods. Nuclear extracts were purified from the cells using lysis buffer (10 mM Hepes-KOH pH 7.8, 10 mM KCl, and 10 mM EDTA, pH 8.0), incubated with specific probes for NF-κB or ISRE DNA-binding sites, electrophoresed, and visualized by autoradiography.

Luciferase Assay. MEFs were transiently transfected with a reporter construct containing the IFN-β promoter together with an empty vector (Mock) or expression constructs for several genes using Lipofectamine 2000. As an internal control, the cells were transfected with a *Renilla* luciferase construct. The transfected cells were left untreated (medium alone) or infected with EMCV for 8 h. The cells were then lysed and subjected to a luciferase assay using a dual-luciferase reporter assay system (Promega) according to the manufacturer's instructions.

Retroviral Expression. Murine LGP2 and LGP2K30A cDNAs were individually cloned into the pLZR-IRES/GFP retroviral vector (30). Retroviruses were produced by transient transfection of the constructs into PlatE cells. MEFs were separately infected with the retroviruses expressing LGP2 and LGP2 (K30A). At 2 days after infection, the cells were exposed to EMCV for 24 h, and the IFN-β concentrations in the culture supernatants were measured by ELISA.

Plaque Assay. At 48 h after EMCV infection, hearts were prepared and homogenized in PBS. The virus titers in the hearts were determined by a standard plaque assay as described previously (9). After centrifugation, the supernatants were serially diluted and added to plates containing HeLa cells. Cells were overlaid with DMEM containing 1% low-melting point agarose and incubated for 48 h. The numbers of plaques were counted.

Measurement of Cytokine Production. Culture supernatants were collected, and the cytokine concentrations were measured using ELISA kits for IFN-β (PBL Biomedical Laboratories) and IL-6 (R&D Systems) according to the manufacturers' instructions.

Statistical Analysis. The statistical significance of differences between groups was determined by Student's *t* test, and survival curves were analyzed by the log-rank test. Values of $P < 0.05$ were considered to indicate statistical significance.

ACKNOWLEDGMENTS. We thank all of the colleagues in our laboratory, E. Kamada for secretarial assistance, and Y. Fujiwara, M. Kumagai, and R. Abe for technical assistance. We thank Drs. A. Kato and T. Dermody for providing viruses. This work was supported by the Special Coordination Funds of the Japanese Ministry of Education, Culture, Sports, Science and Technology, and grants from the Ministry of Health, Labour and Welfare in Japan, the Global Center of Excellence Program of Japan, and the National Institutes of Health (P01 AI070167).

1. Akira S, Uematsu S, Takeuchi O (2006) Pathogen recognition and innate immunity. *Cell* 124:783–801.
2. Honda K, Takaoka A, Taniguchi T (2006) Type I interferon [corrected] gene induction by the interferon regulatory factor family of transcription factors. *Immunity* 25:349–360.
3. Yoneyama M, Fujita T (2008) Structural mechanism of RNA recognition by the RIG-I-like receptors. *Immunity* 29:178–181.
4. Takeuchi O, Akira S (2009) Innate immunity to virus infection. *Immunol Rev* 227:75–86.
5. Kato H, et al. (2008) Length-dependent recognition of double-stranded ribonucleic acids by retinoic acid-inducible gene-I and melanoma differentiation-associated gene 5. *J Exp Med* 205:1601–1610.
6. Schlee M, et al. (2009) Recognition of 5′ triphosphate by RIG-I helicase requires short blunt double-stranded RNA as contained in panhandle of negative-strand virus. *Immunity* 31: 25–34.
7. Schmidt A, et al. (2009) 5′-triphosphate RNA requires base-paired structures to activate antiviral signaling via RIG-I. *Proc Natl Acad Sci USA* 106:12067–12072.
8. Kato H, et al. (2005) Cell type-specific involvement of RIG-I in antiviral response. *Immunity* 23:19–28.
9. Kato H, et al. (2006) Differential roles of MDA5 and RIG-I helicases in the recognition of RNA viruses. *Nature* 441:101–105.
10. Fredericksen BL, Keller BC, Fornek J, Katze MG, Gale M Jr (2008) Establishment and maintenance of the innate antiviral response to West Nile Virus involves both RIG-I and MDA5 signaling through IPS-1. *J Virol* 82:609–616.
11. Loo YM, et al. (2008) Distinct RIG-I and MDA5 signaling by RNA viruses in innate immunity. *J Virol* 82:335–345.
12. Chiu YH, Macmillan JB, Chen ZJ (2009) RNA polymerase III detects cytosolic DNA and induces type I interferons through the RIG-I pathway. *Cell* 138:576–591.
13. Ablasser A, et al. (2009) RIG-I-dependent sensing of poly(dA:dT) through the induction of an RNA polymerase III-transcribed RNA intermediate. *Nat Immunol* 10: 1065–1072.
14. Takahasi K, et al. (2008) Nonself RNA-sensing mechanism of RIG-I helicase and activation of antiviral immune responses. *Mol Cell* 29:428–440.
15. Myong S, et al. (2009) Cytosolic viral sensor RIG-I is a 5′-triphosphate-dependent translocase on double-stranded RNA. *Science* 323:1070–1074.
16. Kawai T, et al. (2005) IPS-1, an adaptor triggering RIG-I- and Mda5-mediated type I interferon induction. *Nat Immunol* 6:981–988.
17. Yoneyama M, et al. (2005) Shared and unique functions of the DExD/H-box helicases RIG-I, MDA5, and LGP2 in antiviral innate immunity. *J Immunol* 175:2851–2858.
18. Rothenfusser S, et al. (2005) The RNA helicase Lgp2 inhibits TLR-independent sensing of viral replication by retinoic acid-inducible gene-I. *J Immunol* 175:5260–5268.
19. Saito T, et al. (2007) Regulation of innate antiviral defenses through a shared repressor domain in RIG-I and LGP2. *Proc Natl Acad Sci USA* 104:582–587.
20. Komuro A, Horvath CM (2006) RNA- and virus-independent inhibition of antiviral signaling by RNA helicase LGP2. *J Virol* 80:12332–12342.
21. Takahasi K, et al. (2009) Solution structures of cytosolic RNA sensor MDA5 and LGP2 C-terminal domains: Identification of the RNA recognition loop in RIG-I-like receptors. *J Biol Chem* 284:17465–17474.
22. Li X, et al. (2009) The RIG-I-like receptor LGP2 recognizes the termini of double-stranded RNA. *J Biol Chem* 284:13881–13891.
23. Pippig DA, et al. (2009) The regulatory domain of the RIG-I family ATPase LGP2 senses double-stranded RNA. *Nucleic Acids Res* 37:2014–2025.
24. Venkataraman T, et al. (2007) Loss of DExD/H box RNA helicase LGP2 manifests disparate antiviral responses. *J Immunol* 178:6444–6455.
25. Yoneyama M, et al. (2004) The RNA helicase RIG-I has an essential function in double-stranded RNA-induced innate antiviral responses. *Nat Immunol* 5:730–737.
26. Linder P (2006) Dead-box proteins: A family affair—active and passive players in RNP-remodeling. *Nucleic Acids Res* 34:4168–4180.
27. Salonen A, Ahola T, Kääriäinen L (2005) Viral RNA replication in association with cellular membranes. *Curr Top Microbiol Immunol* 285:139–173.
28. Cui S, et al. (2008) The C-terminal regulatory domain is the RNA 5′-triphosphate sensor of RIG-I. *Mol Cell* 29:169–179.
29. Pichlmair A, et al. (2006) RIG-I-mediated antiviral responses to single-stranded RNA bearing 5′-phosphates. *Science* 314:997–1001.
30. Ruiz-Vela A, et al. (2001) Transplanted long-term cultured pre-BI cells expressing calpastatin are resistant to B cell receptor-induced apoptosis. *J Exp Med* 194:247–254.

Vol 458|30 April 2009|doi:10.1038/nature07924

LETTERS

Zc3h12a is an RNase essential for controlling immune responses by regulating mRNA decay

Kazufumi Matsushita[1,3]*, Osamu Takeuchi[1,3]*, Daron M. Standley[2], Yutaro Kumagai[1,3], Tatsukata Kawagoe[1,3], Tohru Miyake[1,3], Takashi Satoh[1,3], Hiroki Kato[1,3], Tohru Tsujimura[4], Haruki Nakamura[5] & Shizuo Akira[1,3]

Toll-like receptors (TLRs) recognize microbial components, and evoke inflammation and immune responses[1–3]. TLR stimulation activates complex gene expression networks that regulate the magnitude and duration of the immune reaction. Here we identify the TLR-inducible gene *Zc3h12a* as an immune response modifier that has an essential role in preventing immune disorders. *Zc3h12a*-deficient mice suffered from severe anaemia, and most died within 12 weeks. *Zc3h12a*$^{-/-}$ mice also showed augmented serum immunoglobulin levels and autoantibody production, together with a greatly increased number of plasma cells, as well as infiltration of plasma cells to the lung. Most *Zc3h12a*$^{-/-}$ splenic T cells showed effector/memory characteristics and produced interferon-γ in response to T-cell receptor stimulation. Macrophages from *Zc3h12a*$^{-/-}$ mice showed highly increased production of interleukin (IL)-6 and IL-12p40 (also known as IL12b), but not TNF, in response to TLR ligands. Although the activation of TLR signalling pathways was normal, *Il6* messenger RNA decay was severely impaired in *Zc3h12a*$^{-/-}$ macrophages. Overexpression of Zc3h12a accelerated *Il6* mRNA degradation via its 3′-untranslated region (UTR), and destabilized RNAs with 3′-UTRs for genes including *Il6*, *Il12p40* and the calcitonin receptor gene *Calcr*. Zc3h12a contains a putative amino-terminal nuclease domain, and the expressed protein had RNase activity, consistent with a role in the decay of *Il6* mRNA. Together, these results indicate that Zc3h12a is an essential RNase that prevents immune disorders by directly controlling the stability of a set of inflammatory genes.

The innate immune responses induced by TLRs are tightly controlled, because aberrant activation of TLR responses is harmful to the host, resulting in inflammatory diseases[1–3]. TLR signalling induces the expression of several genes, although only some of these genes have been functionally characterized as immune response modifiers. Therefore, investigation of TLR-inducible genes is important for clarifying the control mechanisms of innate immune reactions. To examine TLR-induced gene expression comprehensively, we performed microarray analysis using mouse macrophages from wild-type, *Myd88*$^{-/-}$ and *Trif*$^{-/-}$ (also known as *Ticam1*$^{-/-}$) mice stimulated with lipopolysaccharide (LPS), a TLR4 ligand. We selected 214 genes in which the expression was induced more than twofold either at 1 or 4 h after stimulation in wild-type cells. Hierarchical clustering of these LPS-inducible genes showed that they could be classified into three major clusters (Supplementary Fig. 1a). Among the clusters, genes in cluster III were rapidly induced in a MyD88-dependent manner. This cluster contained, among others, *Tnf*, *Nfkbiz* and *Zfp36*. Cluster III also contained the gene encoding Zc3h12a (Supplementary Fig. 1b). Northern blot analysis confirmed that *Zc3h12a* mRNA was rapidly induced in mouse macrophages after LPS stimulation and gradually decreased with time (Supplementary Fig. 1c). Zc3h12a has a CCCH-type zinc-finger motif, and forms a family with the homologous proteins Zc3h12b, Zc3h12c and Zc3h12d. Fractionation experiments showed that the Zc3h12a protein is mainly localized in the cytoplasm, rather than in the nucleus (Supplementary Fig. 1d).

To investigate the functional roles of Zc3h12a in the control of immune responses *in vivo*, we generated *Zc3h12a*-deficient mice (Supplementary Fig. 2a and 2b). PCR with reverse transcription (RT–PCR) analysis confirmed that the expression of *Zc3h12a* was abrogated in *Zc3h12a*$^{-/-}$ macrophages (Supplementary Fig. 2c). Although *Zc3h12a*$^{-/-}$ mice are born in a Mendelian ratio, they showed growth retardation, and most of the mice spontaneously died within 12 weeks of birth (Fig. 1a). *Zc3h12a*$^{-/-}$ mice showed severe splenomegaly and lymphoadenopathy (Fig. 1b). Histological examination revealed infiltration of plasma cells in the lung, paraepithelium of the bile duct and pancreas (Fig. 1c and Supplementary Fig. 3). Plasma cells also accumulated in *Zc3h12a*$^{-/-}$ lymph nodes and spleens (Fig. 1c). In the lymph nodes, granuloma formation was observed leading to the generation of giant cells with fused macrophages. Nevertheless, inflammatory changes were not observed in either the intestine or the joints of *Zc3h12a*$^{-/-}$ mice (data not shown).

Zc3h12a$^{-/-}$ mice suffered from severe anaemia, together with an increase in white blood cells and platelets (Fig. 1d). Furthermore, *Zc3h12a*$^{-/-}$ mice developed hyperimmunoglobulinemia of all immunoglobulin isotypes tested (Fig. 1e), and plasma cells infiltrated in the lung interstitial tissues were readily stained with anti-IgG or anti-IgA antibodies (Fig. 1g). Production of anti-nuclear antibodies and anti-double-stranded-DNA antibodies were detected in *Zc3h12a*$^{-/-}$ mice (Fig. 1f). Flow cytometric analysis showed that about 70% of CD19$^+$ B cells were IgM$^-$ IgD$^-$, but immunoglobulin$^+$, indicating that most *Zc3h12a*$^{-/-}$ B cells underwent a class switch in the spleen (Fig. 2a and data not shown). Furthermore, CD138$^+$ CD19^{dull} plasma cells were abundant in the spleen of *Zc3h12a*$^{-/-}$ mice (Fig. 2b). In addition, the expression of CD69 was upregulated in splenic CD3$^+$ T cells, and CD44^{high}CD62L$^-$ T cells accumulated in the periphery (Fig. 2c and Supplementary Fig. 4a). Nevertheless, the proportion of CD4$^+$ Foxp3$^+$ regulatory T cells was comparable between wild-type and *Zc3h12a*$^{-/-}$ mice (Supplementary Fig. 4b). Stimulation of splenic T cells with anti-CD3 antibody resulted in increased production of IFN-γ, but not IL-17 (Fig. 2d and Supplementary Fig. 4c). Ter119$^+$ (also known as Ly76$^+$) erythroblast population was higher in *Zc3h12a*$^{-/-}$ spleens, probably reflecting the responses to anaemia (Supplementary Fig. 4d). However, the ratios of B to T cells and of CD4$^+$ to CD8$^+$ cells were not altered in *Zc3h12a*$^{-/-}$ spleens (Supplementary Fig. 4e, f). To examine whether haematopoietic cells are sufficient for the development of disease, we transferred bone marrow cells from *Zc3h12a*$^{-/-}$ mice to recipient

[1]Laboratory of Host Defense, [2]Laboratory of Systems Immunology, WPI Immunology Frontier Research Center, [3]Research Institute for Microbial Diseases, Osaka University, 3-1 Yamada-oka, Suita, Osaka 565-0871, Japan. [4]Department of Pathology, Hyogo College of Medicine, 1-1 Mukogawa-cho, Nishinomiya, Hyogo 663-8501, Japan. [5]Research Center for Structural and Functional Proteomics, Institute for Protein Research, Osaka University, 3-2 Yamada-oka, Suita, Osaka 565-0871, Japan.
*These authors contributed equally to this work.

©2009 Macmillan Publishers Limited. All rights reserved

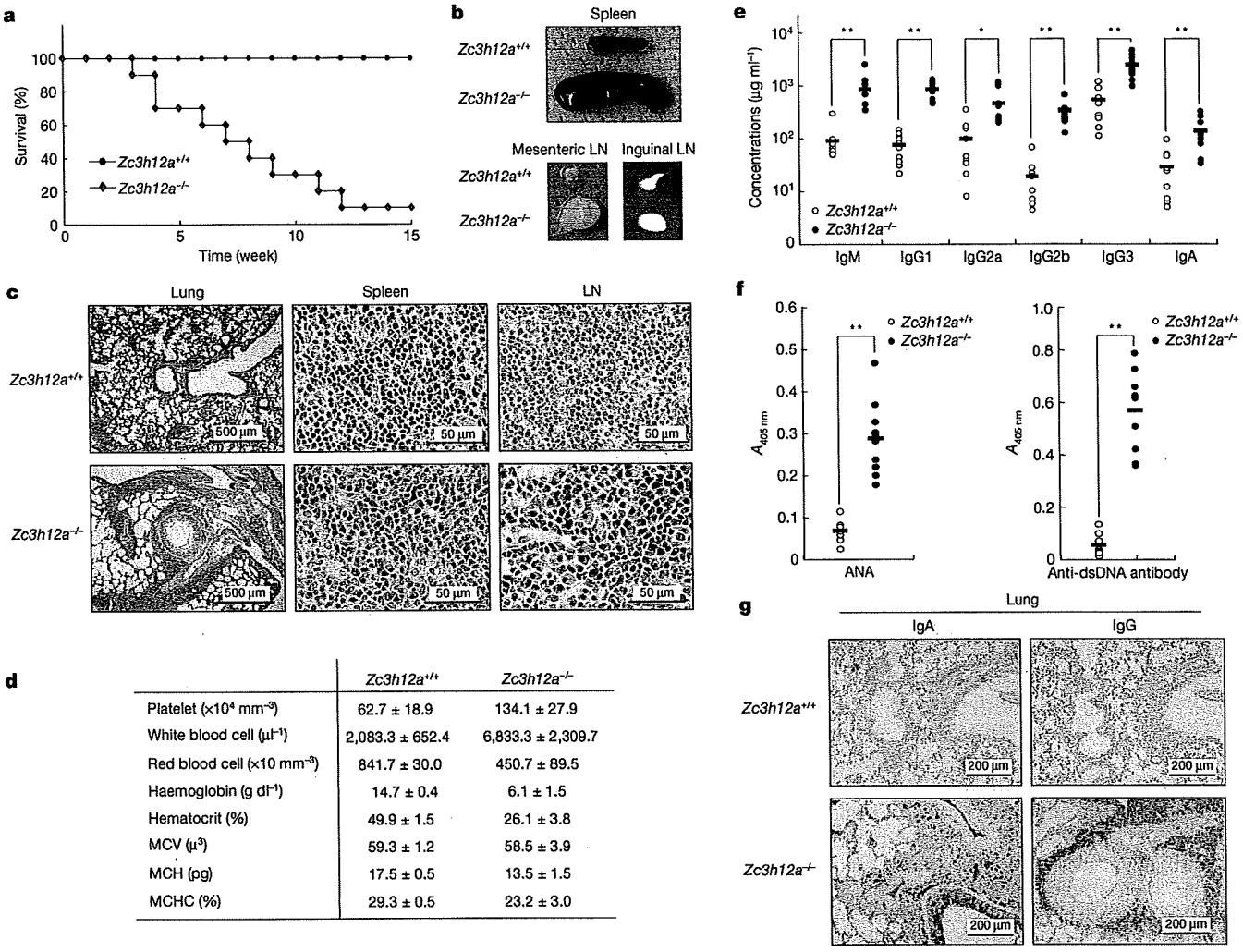

d

	Zc3h12a$^{+/+}$	*Zc3h12a*$^{-/-}$
Platelet (×10^4 mm^{-3})	62.7 ± 18.9	134.1 ± 27.9
White blood cell (μl^{-1})	2,083.3 ± 652.4	6,833.3 ± 2,309.7
Red blood cell (×10 mm^{-3})	841.7 ± 30.0	450.7 ± 89.5
Haemoglobin (g dl^{-1})	14.7 ± 0.4	6.1 ± 1.5
Hematocrit (%)	49.9 ± 1.5	26.1 ± 3.8
MCV (μ^3)	59.3 ± 1.2	58.5 ± 3.9
MCH (pg)	17.5 ± 0.5	13.5 ± 1.5
MCHC (%)	29.3 ± 0.5	23.2 ± 3.0

Figure 1 | Early onset of fetal autoimmune disease in *Zc3h12a*$^{-/-}$ mice. **a**, Survival rates of wild-type (*Zc3h12a*$^{+/+}$) and *Zc3h12a*$^{-/-}$ mice at indicated time periods ($n = 10$). **b**, Gross appearance of spleens and mesenteric and inguinal lymph nodes (LN) from wild-type and *Zc3h12a*$^{-/-}$ mice. **c**, Histology of lung, spleen and lymph nodes from wild-type and *Zc3h12a*$^{-/-}$ mice. **d**, Examination of blood cells. Data are mean ± s.d. of six samples. **e**, Hypergammaglobulinemia in *Zc3h12a*$^{-/-}$ mice. Serum immunoglobulin levels are shown. **f**, Production of anti-nuclear antibodies (ANA) and anti-double-stranded DNA (anti-dsDNA) antibodies in *Zc3h12a*$^{-/-}$ mice. Statistical significance in **e** and **f** was determined using the Student's *t*-test. $*P < 0.05$, $**P < 0.01$. **g**, Immunohistochemistry of lung sections stained with anti-IgG and anti-IgA antibodies.

C57BL/6 mice. *Zc3h12a*$^{-/-}$ bone marrow chimaeras showed delayed, but marked, development of lymphadenopathy and accumulation of plasma cells and CD44^{high}CD62L$^-$ T cells, indicating that haematopoietic cells contribute to the development of immune disorders (Supplementary Fig. 5).

Taken together, these results demonstrate that Zc3h12a is essential for preventing the development of severe immune diseases characterized by an increase in immunoglobulin-producing plasma cells and the formation of granulomas.

We then examined cytokine production from macrophages. As shown in Fig. 2e, stimulation with TLR ligands, MALP-2 (TLR2), poly(I:C) (TLR3), LPS (TLR4), R-848 (TLR7) and CpG-DNA (TLR9), induced increased production of IL-6 and IL-12p40, but not of TNF, in *Zc3h12a*$^{-/-}$ macrophages. Northern blot analysis showed that *Il6* mRNA, but not *Tnf*, *Cxcl1* or *Nfkbia* mRNA, increased significantly in response to LPS in *Zc3h12a*$^{-/-}$ macrophages, (Fig. 2f). We then performed microarray analysis to assess the difference in LPS-inducible gene expression in wild-type and *Zc3h12a*$^{-/-}$ macrophages. Microarray analysis of LPS-inducible genes in macrophages showed that most LPS-inducible genes were comparably expressed in wild-type and *Zc3h12a*$^{-/-}$ cells (Supplementary Fig. 6). Nevertheless, a particular set of genes was highly expressed in *Zc3h12a*$^{-/-}$ macrophages. These included *Il6*, *Ifng*, *Calcr* and *Sprr2d* (Fig. 2g). No differences were observed in the activation of NF-κB or the activator protein 1 (AP-1) by LPS between wild-type and *Zc3h12a*$^{-/-}$ macrophages, indicating that Zc3h12a is not involved in the regulation of the initial TLR signalling pathways (Supplementary Fig. 7).

CCCH-type zinc-finger proteins have been implicated in mRNA metabolism such as mRNA splicing, polyadenylation and the regulation of mRNA decay[4–6]. Thus, we proposed that Zc3h12a might be involved in the destabilization of mRNA, and we examined this possibility using *Il6* as an example. Wild-type and *Zc3h12a*$^{-/-}$ macrophages were stimulated with LPS for 2 h followed by actinomycin D treatment. The half-life of *Il6* mRNA, but not of *Tnf* or *Cxcl1* mRNA, increased in *Zc3h12a*$^{-/-}$ macrophages compared to wild-type cells (Fig. 3a, b). These results indicate that Zc3h12a regulates *Il6* mRNA post-transcriptionally. To determine whether Zc3h12a expression controls *Il6* mRNA, we transfected HEK293 cells stably expressing the tetracycline repressor protein fused to the transactivation domain of the viral transcription factor VP-16 (Tet-off 293 cells), with a plasmid containing the *Il6* coding sequence (CDS) with the 3′-UTR sequence under the control of a tetracycline-responsive promoter (TRE) (pTREtight-Il6-CDS + 3′-UTR). Treatment with doxycycline (dox) terminated the transcription of *Il6* mRNA, and the mRNA decayed in an incubation time-dependent manner (Fig. 3c).

©2009 Macmillan Publishers Limited. All rights reserved

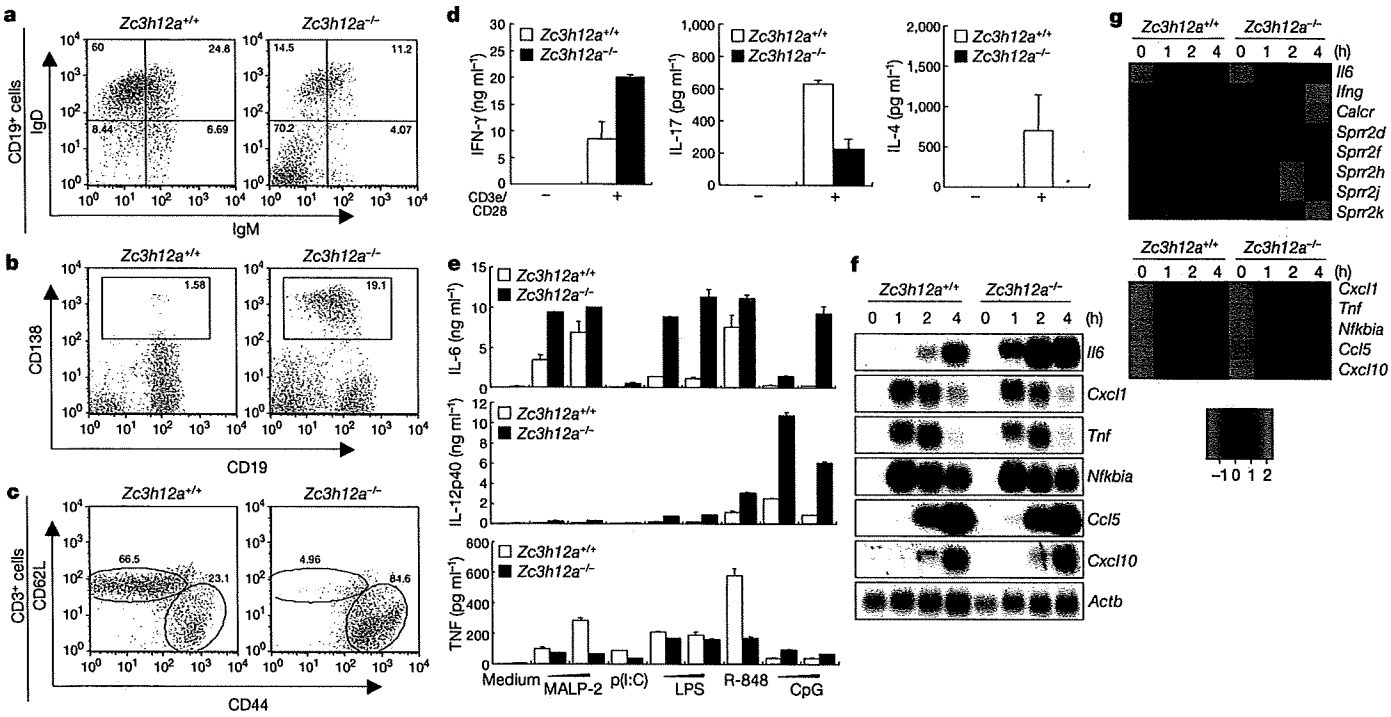

Figure 2 | Cellular abnormalities and augmented cytokine production in *Zc3h12a*$^{-/-}$ mice. **a–c**, Flow cytometric analysis of splenoctytes. Expression of IgM and IgD in splenic CD19^{+} B cells (**a**), the proportion of plasma cells (CD138, also known as Sdc1, and CD19) in the spleen (**b**), and expression of CD62L (also known as Sell) and CD44 in splenic T cells (**c**). Similar results were obtained in three independent experiments. **d**, Production of IFN-γ, IL-17 and IL-4 in response to CD3e and CD28 stimulation in splenic T cells. Error bars indicate s.d. of duplicates. Similar results were obtained in three independent experiments. **e**, Peritoneal macrophages from wild-type and *Zc3h12a*$^{-/-}$ mice were stimulated with MALP-2 (1, 10 ng ml^{-1}), poly(I:C) (p(I:C), 100 μg ml^{-1}), LPS (10, 100 ng ml^{-1}), R-848 (10 nM) and CpG-DNA (0.1, 1 μM) for 24 h. The concentrations of IL-6, IL-12p40 and TNF in the culture supernatants were measured by ELISAs. Error bars indicate the s.d. of duplicates. Similar results were obtained in three independent experiments. **f**, Total RNA from macrophages stimulated with LPS (100 ng ml^{-1}) for indicated periods was extracted and subjected to northern blotting for the expression of *Il6*, *Cxcl1*, *Tnf*, *Nfkbia*, *Ccl5*, *Cxcl10* and β-actin (*Actb*). **g**, Heat map representation of the expression of selected LPS-inducible genes on the basis of microarray analysis of wild-type and *Zc3h12a*$^{-/-}$ peritoneal macrophages.

Overexpression of Zc3h12a greatly accelerated the degradation of *Il6* mRNA (Fig. 3c, d). In contrast, Zc3h12a did not affect the expression of mRNA harbouring the *Il6* CDS without the 3′-UTR sequence (pTREtight-Il6-CDS) (Fig. 3c, d).

Mouse *Il6* mRNA contains five adenine-uridine-rich elements (AREs) in its 3′-UTR (Fig. 3e)[7]. In addition, a conserved element between species comprising about 30 nucleotides was reported to be important for *Il6* mRNA destabilization[8]. To investigate regions of the *Il6* 3′-UTR that are critical for conferring Zc3h12a responsiveness, we used a series of luciferase reporter constructs (pGL3) containing several regions of the *Il6* 3′-UTR (Fig. 3e). When full-length *Il6* 3′-UTR (1–403) was inserted into the reporter, the luciferase activity decreased compared to the luciferase reporter alone. Co-expression of Zc3h12a further reduced the luciferase activity of pGL3-Il6 3′-UTR (1–403) (Fig. 3f). Whereas the luciferase activities of pGL3-Il6 3′-UTR (1–70) and pGL3-Il6 3′-UTR (172–403) were not altered by the expression of Zc3h12a, the luciferase activity of pGL3-Il6 3′-UTR (56–173) decreased in the presence of Zc3h12a. *Il6* 3′-UTR (56–173) contains two AREs and the conserved element (Fig. 3f). By using a set of luciferase reporter constructs with shortened *Il6* 3′-UTRs, we found that the conserved element, but not the ARE, of *Il6* 3′-UTR was important for destabilization by Zc3h12a (Fig. 3f and Supplementary Fig. 8). Although the luciferase activity of pGL3-β-globin 3′-UTR was not affected by Zc3h12a expression, addition of the conserved element of *Il6* 3′-UTR (77–108) to β-globin 3′-UTR conferred a response to Zc3h12a (Fig. 3g). The expression of Zc3h12a reduced the luciferase activity of reporters with the 3′-UTR for *Il12p40* or calcitonin receptor (*Calcr*), but not those with the 3′-UTR of *Ifng* (Fig. 3h), indicating that *Il6*, *Il12p40* and *Calcr* mRNAs are directly regulated by Zc3h12a. IFN-γ might be secondarily regulated by the overproduction of IL-12.

We next examined whether Zc3h12a directly associates with RNA. Synthesized Zc3h12a protein, but not bovine serum albumin (BSA), associates with *Il6* 3′-UTR (1–403) RNA transcribed *in vitro*, indicating that Zc3h12a harbours an RNA-binding capacity (Fig. 4a).

Furthermore, we tested whether the CCCH sequence of Zc3h12a is critical for its role in *Il6* mRNA decay. The expression of Zc3h12a containing the C306R mutation in the CCCH zinc-finger domain, and Zc3h12a without the CCCH domain (lacking amino acids 306–322), could still destabilize *Il6* mRNA (Fig. 4b, c), although these mutant proteins had a reduced ability to degrade *Il6* mRNA when low amounts of proteins were expressed (Supplementary Fig. 9). These results indicate that the CCCH motif plays a part in the control of *Il6* mRNA decay.

The above result prompted us to look for another domain(s) responsible for mRNA decay. Sequence alignment indicated that a conserved N-terminal domain (139–297) in Zc3h12a, just preceding the zinc-finger domain (300–324), shares remote homology to the PilT N-terminus (PIN) domain-like Structural Classification of Proteins (SCOP) superfamily (Fig. 4d). Structural modelling, followed by alignment to other PIN domain structures, revealed a conserved, negatively charged pocket—formed by Asp 141, Asn 144, Asp 226, Asp 244 and Asp 248—that is potentially important for magnesium binding and enzymatic activity (Fig. 4d, e). We proposed that the N-terminal domain of the Zc3h12a protein might be an RNase, and synthesized Zc3h12a protein showed RNase activity for *Il6* 3′-UTR (1–403) mRNA in an Mg^{2+}-dependent manner (Fig. 4f, g). Zc3h12a degraded 5′- and 3′-labelled RNA with similar kinetics, suggesting that Zc3h12a has endonuclease activity (Supplementary Fig. 10). The activity of Zc3h12a seemed to be largely sequence-independent *in vitro*, because target RNAs with various sequences were degraded almost completely (data not shown). Furthermore, the Zc3h12a(D141N) mutant did not

©2009 Macmillan Publishers Limited. All rights reserved

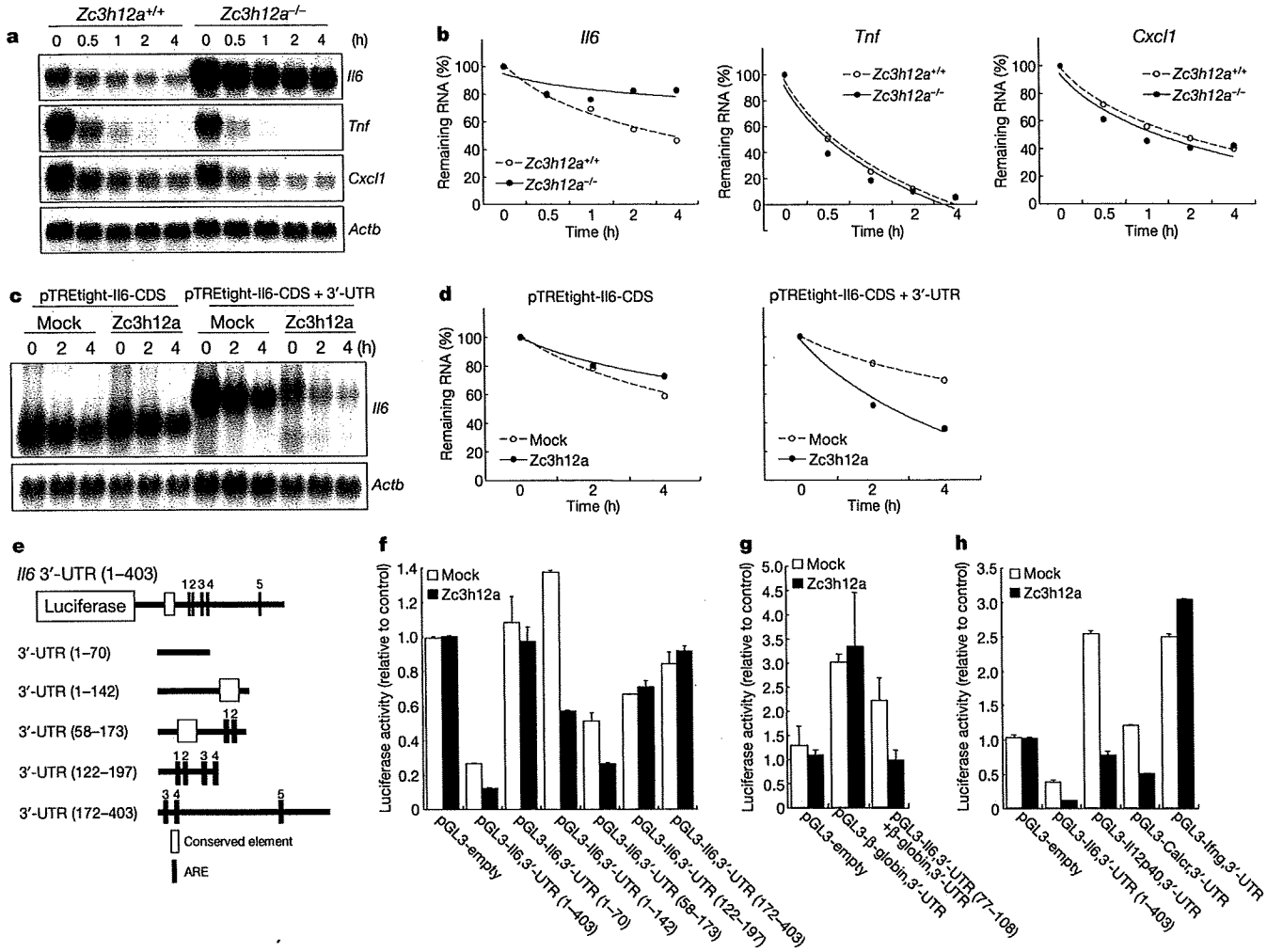

Figure 3 | Zc3h12a destabilizes mRNA from a set of genes through their 3′-UTRs. a, b, Peritoneal macrophages were treated with LPS (100 ng ml^{-1}) for 120 min and then treated with actinomycin D (2 μg ml^{-1}) for the indicated times. Total RNA (10 μg) was extracted and subjected to RNA blot analysis for the expression of *Il6*, *Tnf*, *Cxcl1* and β-actin (*Actb*) probes (**a**). Similar results were obtained in three independent experiments. The autoradiograph was quantified and the ratio of *Il6*, *Tnf* and *Cxcl1* to *Actb* was used to determine the remaining mRNA levels (**b**). **c, d,** HEK293 Tet-off cells were cotransfected with pTREtight-Il6-CDS or pTREtight-Il6-CDS + 3′-UTR, together with the Zc3h12a expression plasmid or control (empty) plasmid. Cells were divided 3 h after transfection and incubated overnight. Total RNA was prepared after dox (1 μg ml^{-1}) treatment, and *Il6* and *Actb* levels were determined by northern blot analysis (**c**). The autoradiograph was quantified and the ratio of *Il6* to *Actb* was used to determine remaining mRNA levels (**d**). **e–g,** Determination of Zc3h12a responsive regions in the *Il6* 3′-UTR. Schematic presentation of *Il6* 3′-UTR and its deletion constructs (**e**). HEK293 cells were transfected with the indicated pGL3 plasmids containing various sequences of *Il6* 3′-UTR (**f**) and β-globin 3′-UTR (**g**), together with the Zc3h12a expression plasmid or control (empty) plasmid. The luciferase activity was determined after 48 h. **h,** HEK293 cells were transfected with pGL3 harbouring the 3′-UTR for *Il6*, *Il12p40*, *Calcr* or *Ifng*, together with the Zc3h12a expression plasmid or control (empty) plasmid and the luciferase activity was determined after 48 h. Error bars indicate the s.d. of duplicates. Similar results were obtained in three independent experiments.

degrade RNA, indicating that the conserved pocket indeed functions as an RNase active site (Fig. 4f, h). The Zc3h12a(D141N) mutant failed to destabilize RNA containing the *Il6* 3′-UTR, indicating that the RNase activity is essential for the function of Zc3h12a (Fig. 4c, i).

This study clearly demonstrates that Zc3h12a is essential for the inhibition of the development of severe autoimmune responses culminating in the lethality of mice. Production of IL-6 and IL-12p40, but not TNF, was increased in *Zc3h12a*$^{-/-}$ macrophages due to mRNA decay failure. CCCH-type zinc-finger proteins have been shown to control mRNA decay by associating with the 3′-UTR. For example, tristetraprolin (Ttp, also known as Zfp36) and its homologues Zfp36l1, Zfp36l2 and Zfp36l3, are critical for the decay of the mRNAs for TNF, GM-CSF, CXCL1 and so on[4,9]. Aged *Ttp*$^{-/-}$ mice develop autoimmune arthritis owing to TNF production[10]. However, to our knowledge, there is no report showing that *Ttp*$^{-/-}$ cells produce increased amounts of IL-6 in response to TLR stimulation. Interestingly, the loss of Zc3h12a did not affect the expression of *Tnf* mRNA in macrophages, indicating that Ttp and Zc3h12a control mRNA decay for different cytokines. Zc3h12a targeted RNA sequences other than AREs, and the IL-6 AREs seem to be regulated by an unknown Zc3h12a-independent mechanism. Considering the profound pathological findings observed in *Zc3h12a*$^{-/-}$ mice, genes other than *Il6* and *Il12p40* are probably critically involved in the pathogenesis too. Identification of Zc3h12a target genes in response to other stimuli or in other cell types will improve our knowledge of the whole mechanism of abnormalities observed in *Zc3h12a*$^{-/-}$ mice. Zc3h12a was recently reported to be a monocyte chemotactic protein-1 (MCP-1)-induced protein[11], and overexpression of Zc3h12a protein was shown to suppress cytokine production in macrophages through inhibition of NF-κB activation[12]. However, the present study shows that Zc3h12a is involved in mRNA decay, but not in TNF regulation, inconsistent with this report.

The Zc3h12a protein has intrinsic RNase activity responsible for the decay of *Il6* mRNA. The mechanism is unique compared to the regulation of other ARE-mediated mRNA decay pathways. For instance, Ttp has been shown to recruit deadenylases for removing polyA tails, facilitating the subsequent degradation of target mRNAs

©2009 Macmillan Publishers Limited. All rights reserved

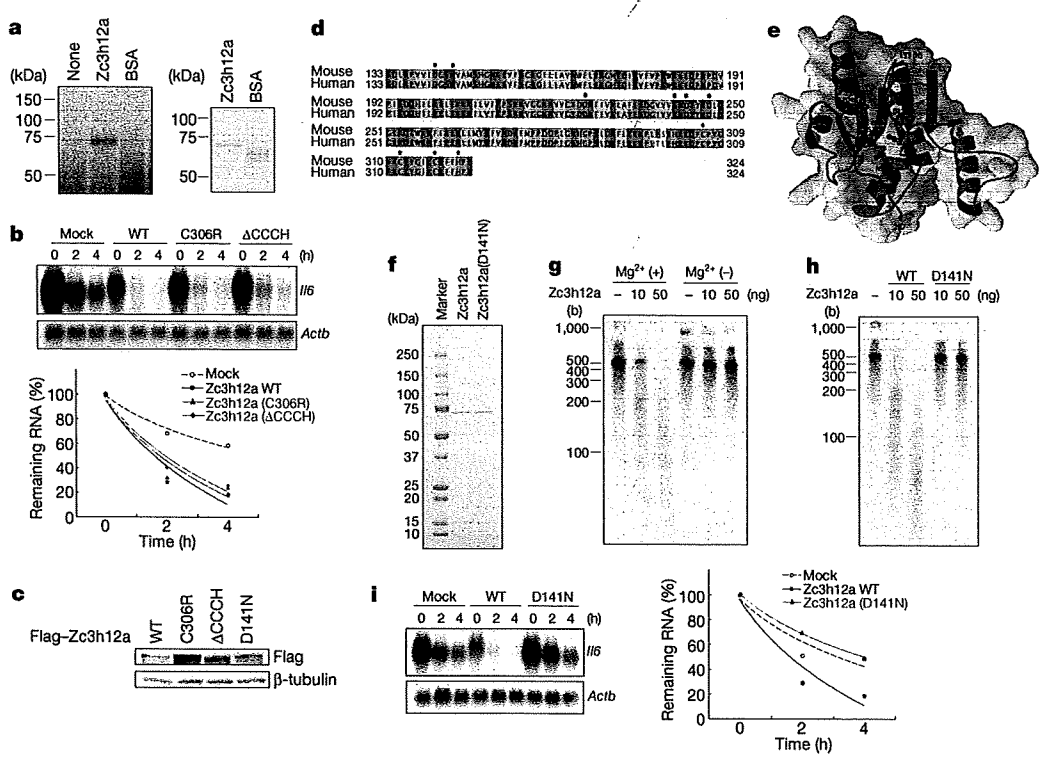

Figure 4 | Zc3h12a contains RNase activity essential for destabilizing *Il6* mRNA. a, Binding of Zc3h12a, but not BSA, to *Il6* 3′-UTR (1–403) mRNA by an ultraviolet cross-linking assay. **b**, Role of CCCH zinc-finger motif in destabilizing *Il6* mRNA. HEK293 Tet-off cells were cotransfected with pTREtight-Il6-CDS + 3′-UTR, together with expression plasmids encoding Flag–Zc3h12a and its mutants (C306R and ΔCCCH). Then cells were treated with dox for the indicated periods and *Il6* expression was determined by northern blot analysis (top). The autoradiograph was quantified and the ratio of *Il6* to *Actb* was used to determine remaining mRNA levels (bottom). WT, wild type. **c**, Expression levels of Zc3h12a mutant proteins determined by immunoblot. **d**, Alignment of N-terminal and CCCH domains in mouse and human Zc3h12a. **e**, The structural model of the Zc3h12a N-terminal domain. **f–h**, Zc3h12a possesses RNase activity. The expression levels of synthesized Zc3h12a and Zc3h12a(D141N) are shown (**f**). The RNase activity of Zc3h12a in degrading *Il6* 3′-UTR mRNA (1–403) in the presence or absence of 5 mM Mg^{2+} (**g**). The RNase activity of Zc3h12a and Zc3h12a(D141N) proteins (**h**). Synthesized RNA was incubated with increasing amounts of indicated proteins. RNA size marker is indicated in the left; 'b' denotes bases. **i**, HEK293 Tet-off cells were cotransfected with pTREtight-Il6 full and Zc3h12a(D141N). The cells were then treated with dox for the indicated periods and *Il6* expression was determined by northern blot analysis.

by exonucleases[4]. Thus, it is intriguing that Zc3h12a has endonuclease activity, which, at least *in vitro*, does not show sequence specificity. The target specificity may be determined by binding partner(s) of Zc3h12a, or Zc3h12a may have a preferential sequence for degradation under certain conditions. The mechanism of how Zc3h12a induces decay of mRNAs is an intriguing topic for further exploration. The RNase domain is conserved in four Zc3h12 family members, and the homologues of this protein family are found in metazoans such as *Drosophila melanogaster* (NCBI accession number CG10889) and *Caenorhabditis elegans* (NCBI accession number C30F12.1). Thus, regulation of mRNA by the RNase domain and CCCH zinc-finger domain seems to be evolutionally conserved.

Another RING-type ubiquitin ligase protein containing a CCCH zinc-finger motif called roquin (also known as Rc3h1) is essential for suppressing autoimmunity by controlling expression of the ICOS costimulatory molecule[13]. Roquin and several microRNAs seem to share an *Icos* 3′-UTR RNA segment for suppressing its degradation[14]. Given that each CCCH zinc-finger protein seems to have target mRNA specificity and 60 CCCH-type zinc-finger proteins have been identified in the mammalian genome[15], control of mRNA decay might be as important as the control of transcription in terms of regulation of innate immune responses. Future studies on CCCH zinc-finger proteins will be important for understanding the mechanisms of immune regulation by the control of mRNAs.

METHODS SUMMARY

Mice, reagents, cells and plasmids. Details are given in Methods.

ELISA. IL-4, IL-6, IL-12p40, IL-17, IFN-γ and TNF in culture supernatants, and mouse ANA in serum, were measured by ELISAs following manufacturer's protocols. ELISAs for mouse IgM, IgG1, IgG2a, IgG2b, IgG3 and anti-double-stranded DNA antibodies in serum were preformed as previously described[16,17].

Northern blotting, immunoblotting and EMSA. Northern blotting, immunoblotting and EMSA were performed as previously described[16].

Determination of haematological values. Haematological analysis of bloods prepared from wild-type and *Zc3h12a*$^{-/-}$ mice were performed at SRL Inc.

Flow cytometry. Details of flow cytometry are given in Methods. Cells were stained with indicated antibodies. The data were then acquired on a FACS Calibur or FACS Canto II flow cytometer (BD Biosciences), and analysed using FlowJo.

Measurement of RNA stability. mRNA stability was determined using three different methods. First, northern blot analysis was performed using total RNAs prepared from *Zc3h12a*$^{-/-}$ macrophages stimulated with LPS for 2 h followed by treating with actinomycin D. Second, the northern blot Tet-off system was used with HEK293 Tet-off cells transfected by pTRE-Il6 plasmids together with pFlag-Zc3h12a plasmids. Third, the luciferase assay of cell lysates prepared from HEK293 cells transfected with pGL3 plasmids together with pFlag-Zc3h12a plasmid was used.

***In vitro* RNA cleavage assay.** Cleavage activities of wild-type and mutant forms of Zc3h12a were analysed as described previously[18]. After incubation of recombinant Zc3h12a proteins with *in vitro* transcribed [^{32}P]-labelled RNAs, the cleaved RNAs were purified and analysed by denaturing PAGE and autoradiography. Details of the cleavage assay, expression of recombinant proteins and synthesis of [^{32}P]-labelled RNAs are given in Methods.

Full Methods and any associated references are available in the online version of the paper at www.nature.com/nature.

Received 23 January; accepted 25 February 2009.
Published online 25 March 2009.

1. Akira, S., Uematsu, S. & Takeuchi, O. Pathogen recognition and innate immunity. *Cell* 124, 783–801 (2006).

©2009 Macmillan Publishers Limited. All rights reserved

2. Beutler, B. *et al.* Genetic analysis of host resistance: Toll-like receptor signaling and immunity at large. *Annu. Rev. Immunol.* **24**, 353–389 (2006).
3. Medzhitov, R. Recognition of microorganisms and activation of the immune response. *Nature* **449**, 819–826 (2007).
4. Anderson, P. Post-transcriptional control of cytokine production. *Nature Immunol.* **9**, 353–359 (2008).
5. Barabino, S. M., Hubner, W., Jenny, A., Minvielle-Sebastia, L. & Keller, W. The 30-kD subunit of mammalian cleavage and polyadenylation specificity factor and its yeast homolog are RNA-binding zinc finger proteins. *Genes Dev.* **11**, 1703–1716 (1997).
6. Kanadia, R. N. *et al.* A muscleblind knockout model for myotonic dystrophy. *Science* **302**, 1978–1980 (2003).
7. Zhao, W., Liu, M. & Kirkwood, K. L. p38α stabilizes interleukin-6 mRNA via multiple AU-rich elements. *J. Biol. Chem.* **283**, 1778–1785 (2008).
8. Paschoud, S. *et al.* Destabilization of interleukin-6 mRNA requires a putative RNA stem-loop structure, an AU-rich element, and the RNA-binding protein AUF1. *Mol. Cell. Biol.* **26**, 8228–8241 (2006).
9. Datta, S. *et al.* Tristetraprolin regulates CXCL1 (KC) mRNA stability. *J. Immunol.* **180**, 2545–2552 (2008).
10. Taylor, G. A. *et al.* A pathogenetic role for TNF-α in the syndrome of cachexia, arthritis, and autoimmunity resulting from tristetraprolin (TTP) deficiency. *Immunity* **4**, 445–454 (1996).
11. Zhou, L. *et al.* Monocyte chemoattractant protein-1 induces a novel transcription factor that causes cardiac myocyte apoptosis and ventricular dysfunction. *Circ. Res.* **98**, 1177–1185 (2006).
12. Liang, J. *et al.* A novel CCCH-zinc finger protein family regulates proinflammatory activation of macrophages. *J. Biol. Chem.* **283**, 6337–6346 (2008).
13. Vinuesa, C. G. *et al.* A RING-type ubiquitin ligase family member required to repress follicular helper T cells and autoimmunity. *Nature* **435**, 452–458 (2005).
14. Yu, D. *et al.* Roquin represses autoimmunity by limiting inducible T-cell co-stimulator messenger RNA. *Nature* **450**, 299–303 (2007).
15. Liang, J., Song, W., Tromp, G., Kolattukudy, P. E. & Fu, M. Genome-wide survey and expression profiling of CCCH-zinc finger family reveals a functional module in macrophage activation. *PLoS One* **3**, e2880 (2008).
16. Sato, S. *et al.* Essential function for the kinase TAK1 in innate and adaptive immune responses. *Nature Immunol.* **6**, 1087–1095 (2005).
17. Fukuyama, H., Nimmerjahn, F. & Ravetch, J. V. The inhibitory Fcγ receptor modulates autoimmunity by limiting the accumulation of immunoglobulin G^+ anti-DNA plasma cells. *Nature Immunol.* **6**, 99–106 (2005).
18. Miyoshi, K., Uejima, H., Nagami-Okada, T., Siomi, H. & Siomi, M. C. *In vitro* RNA cleavage assay for Argonaute-family proteins. *Methods Mol. Biol.* **442**, 29–43 (2008).

Supplementary Information is linked to the online version of the paper at www.nature.com/nature.

Acknowledgements We thank all colleagues in our laboratory, E. Kamada for secretarial assistance, and Y. Fujiwara, M. Kumagai and R. Abe for technical assistance. We thank S. Sato for discussions and W. Zhao and K. Kirkwood for plasmids. This work was supported by the Special Coordination Funds of the Japanese Ministry of Education, Culture, Sports, Science and Technology, grants from the Ministry of Health, Labour and Welfare in Japan, the Global Center of Excellence Program of Japan, and the NIH (P01 AI070167).

Author Contributions K.M. generated *Zc3h12a*$^{-/-}$ mice and performed most experiments. O.T. identified Zc3h12a, designed the research and wrote the paper. D.M.S. and H.N. carried out structural modelling. Y.K. analysed microarray data, and T.T. was responsible for histological analysis. T.K., T.M., T.S. and H.K. helped with experiments. S.A. designed the research and supervised the project.

Author Information Microarray data are deposited in the Gene Expression Omnibus (accession number GSE14890 for series of *Myd88*$^{-/-}$ and *Trif*$^{-/-}$ macrophages, and GSE14891 for series of *Zc3h12a*$^{-/-}$ macrophages). The structure model of Zc3h12a nuclease domain has been deposited in the Protein Model DataBase (PMDB) under accession number PM0075640. Reprints and permissions information is available at www.nature.com/reprints. Correspondence and requests for materials should be addressed to S.A. (sakira@biken.osaka-u.ac.jp).

©2009 Macmillan Publishers Limited. All rights reserved

METHODS

Generation of *Zc3h12a*$^{-/-}$ mice. Genomic DNA containing *Zc3h12a* was isolated from GSI-I embryonic stem cells and characterized by restriction enzyme mapping and sequencing analysis. A targeting vector was designed to replace exon 3 to exon 5 containing the CCCH type zinc-finger domain, with a neomycin-resistance gene. A 1.1-kb ClaI–BamI fragment was used as the 3′ homology, and a 5.9-kb NotI–SalI fragment was used as the 5′ homology region. A total of 30 μg of NotI-linearized vector was electroporated into GSI-I embryonic stem cells. After selection with G418, drug-resistant clones were picked up and screened by PCR and Southern blot analysis. These clones were individually microinjected into blastocysts derived from C57BL/6 mice and transferred to pseudopregnant females. Matings of chimaeric male mice to C57BL/6 female mice resulted in the transmission of the mutant allele to the germ line. Resulting *Zc3h12a*$^{+/-}$ mice were intercrossed to generate *Zc3h12a*$^{-/-}$ mice. All animal experiments were done with the approval of the Animal Research Committee of the Research Institute for Microbial Diseases (Osaka University).

Reagents and cells. ELISA kits for mouse IL-4, IL-6, IL-12p40, IL-17, IFN-γ and TNF were purchased from R&D systems. The mouse ANA antibody ELISA kit was purchased from Alpha Diagnostic. Monoclonal anti-YY1 (H-10) and HRP-conjugated monoclonal anti-β-tubulin (D-10) antibodies were obtained from SantaCruz. HRP-conjugated anti-Flag antibody was purchased from Sigma. TLR ligands, including MALP-2, poly(I:C), LPS from *Salmonella Minnesota* Re595, R-848 and CpG oligonucleotide (ODN1668) were obtained as described previously[19].

Peritoneal exudate cells were isolated from the peritoneal cavities of mice 3 days after injection with 2 ml of 4.0% thioglycollate medium (Sigma) by washing with ice-cold Hank's buffered salt solution (Invitrogen). The HEK293 Tet-off cell line was purchased from Clontech.

Plasmids. *Zc3h12a* cDNA was inserted into a pFlag-CMV2 vector (Invitrogen). Point mutations (C306R and D141N) and deletion of the CCCH domain were carried out using the above-mentioned plasmid using QuickChangeII Site-Directed Mutagenesis Kit (Stratagene). pGL3 vector containing full-length (1–403) or parts (1–70, 58–173, 172–403) of *Il6* 3′-UTR sequences were supplied by W. Zhao and K. Kirkwood[7]. Parts (1–92, 1–102, 1–112, 1–132, 1–142 and 122–197) of *Il6* 3′-UTR cDNA were inserted in the pGL3 vector. 3′-UTR cDNA of β-globin (1–130) with or without *Il6* 3′-UTR (77–108) sequence, and the 3′-UTR cDNAs of *Il12p40* (1–781), *Calcr* (1–1601) and *Ifng* (1–631) were inserted in the pGL3 vector. *Il6* CDS and *Il6* CDS + 3′-UTR were inserted in pTREtight vector (Clontech). Wild-type and mutant (D141N) *Zc3h12a* cDNA were inserted in the pGEX-6P1 vector (GE Healthcare). *Il6* 3′-UTR cDNA was inserted downstream of the T7 promoter of pBluescript.

Flow cytometry. Antibodies for flow cytometry were purchased from BD Biosciences. Cell suspensions of spleen were prepared by sieving and gentle pipetting. For surface staining, cells were maintained in the dark at 4 °C throughout. Cells were washed in ice-cold FACS buffer (2% FCS, 0.02% NaN_3 in PBS), then incubated with each antibody for 15 min and washed twice with FACS buffer. Foxp3$^+$ regulatory T cell was stained using Mouse Regulatory T Cell Staining Kit (eBioscience) following the manufacturer's instructions. Intracellular cytokines were stained using Cytofix/Cytoparm Plus Fixation/Permeabilization Kit (BD Biosciences) following the manufacturer's instructions. Data were acquired on a FACS Calibur or FACS Canto II flow cytometer (BD Biosciences), and analysed using FlowJo.

Stability of mRNA in macrophages. Peritoneal macrophages (1×10^6) from wild-type and *Zc3h12a*$^{-/-}$ mice were stimulated with LPS (100 ng ml^{-1}) for 2 h. Actinomycin D (2 μg ml^{-1}) was then added to the culture medium to stop transcription, and total RNAs were prepared at the indicated time periods. The RNAs were subjected to northern blot analysis to determine *Il6*, *Tnf*, *Cxcl1* and *Actb* mRNA levels.

The Tet-off system. HEK293 Tet-off cells (3×10^6) were transfected with pTREtight-Il6-CDS (which have an *Il6* coding sequence) or pTREtight-Il6-CDS + 3′-UTR (which have a *Il6* coding and non-coding 3′-UTR sequence), together with wild-type or mutant forms of Zc3h12a expression plasmids or control (empty) plasmid. After 3 h, the cells were subdivided into three 60-mm dishes and cultured overnight. mRNA transcription from pTREtight vectors were terminated by the addition of dox (1 μg ml^{-1}), and total RNA was prepared at the indicated time periods. The RNA was subjected to northern blot analysis to determine *Il6* and *Actb* mRNA levels.

Luciferase assay. HEK293 cells were transfected with pGL3-Il6 3′-UTR plasmids or pGL3-empty plasmid together with Zc3h12a expression plasmid or empty control plasmid. After 48 h of cultivation, cells were lysed and luciferase activities in the lysates were determined using the Dual-luciferase reporter assay system (Promega). The *Renilla* luciferase gene was simultaneously transfected as an internal control.

Bone marrow transfer. Bone marrow cells were prepared from wild-type and *Zc3h12a*$^{-/-}$ mice. The cells were intravenously injected into lethally irradiated CD45.1 C57BL/6 mice. The chimaeric mice were given neomycin and ampicilin in their drinking water for 4 weeks. The mice were analysed at least 8 weeks after reconstitution. More than 90% of splenocytes from chimaeric mice were CD45.2-positive.

Expression of Zc3h12a protein in bacteria. The proteins were expressed in *Escherichia coli* BL21-Gold(DE3)pLysS (Stratagene) transformed with pGEX-6P1-Zc3h12a or Zc3h12a(D141N) mutant. After expression of the proteins, the cells were collected and resuspended in PBS. The cells were lysed by sonication followed by addition of Triton X-100 at a final concentration of 1% and incubation for 30 min at 4 °C with gentle shaking. The debris were then removed by centrifugation and supernatants were incubated with Glutathione Sepharose 4B (GE Healthcare) for 30 min at 4 °C with gentle shaking. The resins were collected and washed five times with PBS and resuspended in PreScission Protease cleavage buffer (50 mM Tris, 150 mM NaCl, 1 mM EDTA and 1 mM dithiothreitol (DTT)). PreScission Protease (GE Healthcare) (80 U) was added and incubated for 4 h at 4 °C with gentle shaking. Supernatants were collected and stored at −80 °C as purified recombinant protein solutions.

Synthesis of [^{32}P]-labelled RNAs. The pBluescript-Il6 3′-UTR (1–430) plasmid was used as a template for the synthesis of RNA having an *Il6* 3′-UTR sequence. *In vitro* RNA synthesis and [^{32}P] labelling was performed by using Riboprobe in vitro Transcription system (Promega) following manufacturer's instructions. The 5′-end labelling was performed using non-labelled RNA and Kinase Max 5′-end labelling Kit (Ambion) following manufacturer's instructions. The 3′-end labelling was performed by incubation of non-labelled RNA with T4 RNA Ligase (Takara) and [^{32}P]pCp (GE Healthcare).

RNA binding assay. [^{32}P]-labelled RNA (1×10^6 c.p.m.) were mixed with recombinant protein or BSA (Pierce) in a buffer (25 mM HEPES, 50 mM potassium acetate, 5 mM DTT) and incubated for 20 min at room temperature. Heparin was then added at a final concentration of 0.5 μg ml^{-1} and incubated further 10 min. The samples were cross-linked by irradiation with 254-nm ultraviolet light using FUNA-UV-LINKER FS-800 (Funakoshi) at a distance of 5 cm from the light source for 20 min on ice. The cross-linked samples were treated with RNaseT (100 U) for 20 min at room temperature, followed by treatment with RNaseA (1 μg) for 15 min at 37 °C. After the digestion, the proteins bound with [^{32}P]-labelled RNA were analysed by SDS–PAGE and autoradiography.

***In vitro* RNA cleavage assay.** Recombinant proteins and *in vitro* transcribed [^{32}P]-labelled RNAs (5,000 c.p.m.) were mixed in cleavage buffer (25 mM HEPES, 50 mM potassium acetate, 5 mM DTT) with or without 5 mM magnesium acetate[2] in the presence of Rnasin plus (40 U) (Promega). The cleaved RNA was purified with Trizol (Invitrogen) and analysed by denaturing PAGE using 6% TBE–urea gel (Invitrogen) and autoradiography.

Microarray analysis. Peritoneal macrophages from wild-type, *MyD88*$^{-/-}$ and *Trif*$^{-/-}$ mice were stimulated with 100 ng ml^{-1} LPS for 0, 1 and 4 h. Total RNA was extracted with an RNeasy kit (Qiagen), double-stranded cDNA was synthesized from 10 μg of total RNA with the SuperScript Choice System (Invitrogen) primed with T7-(dT) 24 primer. These cDNAs were used to prepare biotin-labelled complementary RNA by an *in vitro* transcription reaction performed using T7 RNA polymerase in the presence of biotinylated ribonucleotides, according to the manufacturer's protocol (Enzo Diagnostics). The cRNA product was purified using an RNeasy kit (Qiagen), fragmented, and hybridized to Affymetrix mouse expression array 430A microarray chips, according to the manufacturer's protocol. For determination of LPS-inducible genes in *Zc3h12a*$^{-/-}$ macrophages, peritoneal macrophages were stimulated with 100 ng ml^{-1} LPS. Total RNA was then extracted with Trizol (Invitrogen Life Technologies) and further purified using an RNeasy kit. Biotin-labelled cDNA was synthesized from 100 ng of the purified RNA using Ovation Biotin RNA Amplification and Labelling System (Nugen) according to the manufacturer's protocol. Hybridization, staining, washing and scanning of Affymetrix mouse Genome 430 2.0 microarray chip was done following the manufacturer's instructions. Robust multichip average (RMA) expression values were calculated using R and Bioconductor affy package. For hierarchical clustering, probes having a more than two- or fivefold increase compared to 0 h after stimulation were selected. The RMA expression values were transformed to fit averages and standard deviations to zero and one, respectively, by each probe. For analysis of LPS-inducible genes in *MyD88*$^{-/-}$ and *Trif*$^{-/-}$ macrophages, distances between probes were calculated using Pearson's correlation coefficient as a distance function. For analysis of LPS inducible genes in *Zc3h12a*$^{-/-}$ macrophages, principle component analysis for RMA values was performed and Euclidean distances between probes were computed using first to fifth principle components. Hierarchical clustering was carried out using these distances with Ward's method. These calculations and generation of heat map representation were carried out using R and Bioconductor.

©2009 Macmillan Publishers Limited. All rights reserved

Immunohistochemistry. The tissues was fixed with 10% formalin neutral buffer solution, embedded in paraffin, and cut into 5-μm thick sections. Sections were heated in Target Retrieval Solution (Dako) at 98 °C for 40 min to facilitate antigen retrieval. The sections were incubated with peroxidase-conjugated goat IgG fraction to mouse IgA (alpha chain) (MP Biomedicals) diluted 1:50 by antibody diluent (ChemMate, Dako), or peroxidase-conjugated goat affinity purified F(ab')2 fragment to mouse IgG (whole molecule) (MP Biomedicals) diluted 1:25 by antibody diluent, for 30 min at room temperature. Immunoreacted cells for mouse IgA and IgG were visualized with diaminobenzidine (Dako). The sections were lightly counterstained with haematoxylin.

Structure modelling. A model of the Zc3h12c N-terminal domain was constructed as follows: first, the sequence was submitted to the BioInfoBank Meta Server (http://bioinfo.pl), and the top ten models were built using default settings. The best model was then chosen by submitting each to the SeSAW functional annotation server (http://pdbjs6.pdbj.org/SeSAW/), and selecting the model with the highest score. The model chosen was built form the structural genomics template 2qip, using the FFAS03 server (http://ffas.ljcrf.edu/ffas-cgi/cgi/ffas.pl) and Modeller[20]. This model, which also had the highest three-dimensional Jury score, contained a cluster of conserved aspartic acids (D141, D226, S242, D244 and D248) that are also conserved in the active sites of Flap endonucleases (for example, Protein Data Bank ID 1UT5)[21]. Electrostatic surfaces were prepared using the *e*F-surf server (http://ef-site.hgc.jp/eF-surf/) and *e*F-site[22].

19. Kawagoe, T. *et al.* Sequential control of Toll-like receptor-dependent responses by IRAK1 and IRAK2. *Nature Immunol.* **9**, 684–691 (2008).
20. Eswar, N. *et al.* Comparative protein structure modeling using MODELLER. *Curr. Protoc. Bioinformatics* **Chapter 5**, Unit 5.6 (2006).
21. Feng, M. *et al.* Roles of divalent metal ions in flap endonuclease-substrate interactions. *Nature Struct. Mol. Biol.* **11**, 450–456 (2004).
22. Kinoshita, K. & Nakamura, H. eF-site and PDBjViewer: database and viewer for protein functional sites. *Bioinformatics* **20**, 1329–1330 (2004).

©2009 Macmillan Publishers Limited. All rights reserved

⌘ Author's Choice

THE JOURNAL OF BIOLOGICAL CHEMISTRY VOL. 284, NO. 20, pp. 13348–13354, May 15, 2009
© 2009 by The American Society for Biochemistry and Molecular Biology, Inc. Printed in the U.S.A.

Identification of Loss of Function Mutations in Human Genes Encoding RIG-I and MDA5

*IMPLICATIONS FOR RESISTANCE TO TYPE I DIABETES**

Received for publication, December 16, 2008, and in revised form, March 25, 2009 Published, JBC Papers in Press, March 26, 2009, DOI 10.1074/jbc.M809449200

Taeko Shigemoto[‡§], Maiko Kageyama[‡§], Reiko Hiral[‡], JiPing Zheng[‡], Mitsutoshi Yoneyama[‡§¶], and Takashi Fujita[‡§1]

From the [‡]Laboratory of Molecular Genetics, Institute for Virus Research, and [§]Laboratory of Molecular Cell Biology, Graduate School of Biostudies, Kyoto University, Kyoto 606-8507 and [¶]PRESTO, Japan Science and Technology Agency, 4-1-8 Honcho Kawaguchi, Saitama 332-0012, Japan

Retinoic acid-inducible gene I (RIG-I) and melanoma differentiation-associated gene 5 (MDA5) are essential for detecting viral RNA and triggering antiviral responses, including production of type I interferon. We analyzed the phenotype of non-synonymous mutants of human RIG-I and MDA5 reported in databases by functional complementation in cell cultures. Of seven missense mutations of RIG-I, S183I, which occurs within the second caspase recruitment domain repeat, inactivated this domain and conferred a dominant inhibitory function. Of 10 mutants of MDA5, two exhibited loss of function. A nonsense mutation, E627*, resulted in deletion of the C-terminal region and double-stranded RNA (dsRNA) binding activity. Another loss of function mutation, I923V, which occurs within the C-terminal domain, did not affect dsRNA binding activity, suggesting a novel and essential role for this residue in the signaling. Remarkably, these mutations are implicated in resistance to type I diabetes. However, the A946T mutation of MDA5, which has been implicated in type I diabetes by previous genetic analyses, affected neither dsRNA binding nor *IFN* gene activation. These results provide new insights into the structure-function relationship of RIG-I-like receptors as well as into human RIG-I-like receptor polymorphisms, antiviral innate immunity, and autoimmune diseases.

Innate and adaptive immune systems constitute the defense against infections by pathogens. Immediately after an infection occurs, various cells in the body sense the virus and initiate antiviral responses in which type I IFN[2] plays a critical role, both in viral inhibition and in the subsequent adaptive immune response (1). The production of IFN is initiated when sensor molecules such as Toll-like receptors (TLRs) and RLRs detect virus-associated molecules. TLRs detect pathogen-associated molecular patterns (PAMPs) at the cell surface or in the endosome in immune cells such as dendritic cells and macrophages (2). RLRs sense viral RNA in the cytoplasm of most cell types and induce antiviral responses, including the activation of *IFN* genes (3). RLRs include RIG-I, MDA5, and laboratory of genetics and physiology 2 (LGP2).

It is proposed that RLRs sense and activate antiviral signals through the coordination of their functional domains (4). The N-terminal region of RIG-I and MDA5 is characterized by two repeats of CARD and functions as an activation domain (3). This domain is responsible for the transduction of signals downstream to IFN-β promoter stimulator 1 (IPS-1) (also known as MAVS, VISA, and Cardif). The primary sequence of the CTD, consisting of ~140 amino acids, is conserved among RLRs. The CTD of RIG-I functions as a viral RNA-sensing domain as revealed by biochemical and structural analyses (5, 6). Both dsRNA and 5′-ppp-ssRNA, which are generated in the cytoplasm of virus-infected cells, are recognized by a basic cleft structure of RIG-I CTD. In addition to its RNA recognition function, the CTD of RIG-I and LGP2 functions as a repression domain through interaction with the activation domain. The repression domain is responsible for keeping RIG-I inactive in non-stimulated cells (3, 7). The helicase domain, with DEXD/H box-containing RNA helicase motifs, is the largest domain found in RLRs. Once dsRNA or 5′-ppp-ssRNA is recognized by the CTD, the helicase domain causes structural changes to release the activation domain. ATP binding and/or its hydrolysis is essential for the conformational change because Walker's ATP-binding site within the helicase domain is essential for signaling by RIG-I and MDA5.

Analyses of knock-out mice have revealed that RIG-I and MDA5 recognize distinct RNA viruses (8, 9). Picornaviruses are detected by MDA5, but many other viruses such as influenza A, Sendai, vesicular stomatitis, and Japanese encephalitis are detected by RIG-I. The difference is based on the distinct non-self RNA patterns generated by viruses, as demonstrated by the finding that RIG-I is selectively activated by dsRNA or 5′-ppp ssRNA, whereas MDA5 is activated by long dsRNA (10–12).

Single nucleotide polymorphisms (SNPs) of the human *RIG-I* and *MDA5* genes including several non-synonymous SNPs (nsSNPs), which potentially alter the function of the proteins encoded, are reported in databases. In this report, we investigated the functions of nsSNPs of RIG-I and MDA5 by functional complementation using respective knock-out cells. We identified

* This work was supported by grants from the Ministry of Education, Culture, Sports, Science and Technology of Japan, Japan Science and Technology Agency, The Mochida Memorial Foundation for Medical Pharmaceutical Research, and Nippon Boehringer Ingelheim.

⌘ *Author's Choice*—Final version full access.

[1] To whom correspondence should be addressed: Laboratory of Molecular Genetics, Institute for Virus Research, Kyoto University, Kyoto 606-8507, Japan. Tel.: 81-75-751-4031; Fax: 81-75-751-4031; E-mail: tfujita@virus.kyoto-u.ac.jp.

[2] The abbreviations used are: IFN, interferon; IPS-1, IFN-β promoter stimulator 1; RIG-I, retinoic acid-inducible gene I; MDA5, melanoma differentiation-associated gene 5; LGP2, laboratory of genetics and physiology 2; TLR, Toll-like receptor; RLR, RIG-I-like receptor; PAMP, pathogen-associated molecular pattern; CARD, caspase recruitment domain; CTD, C-terminal domain; SNP, single nucleotide polymorphisms; nsSNP, non-synonymous SNP; MEF, mouse embryonic fibroblast; SeV, Sendai virus; T1D, type I diabetes; dsRNA, double-stranded RNA; ssRNA, single-stranded RNA; EMSA, electrophoretic mobility shift assay; WT, wild type.

Downloaded from www.jbc.org at OSAKA UNIVERSITY, on March 22, 2010

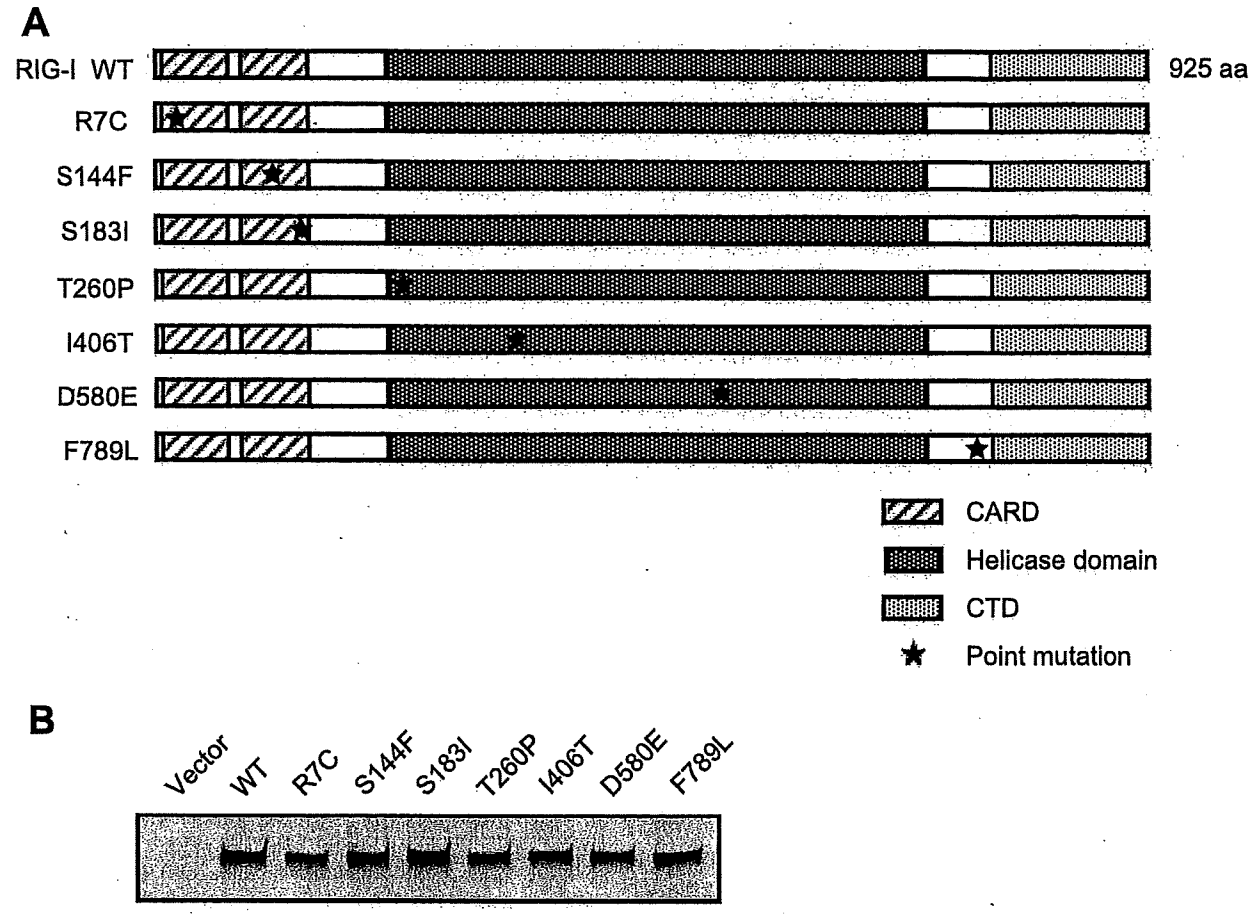

FIGURE 1. **RIG-I nsSNP mutants and their expression in MEFs.** *A*, schematic representation of the RIG-I wild type and nsSNP-containing mutants. RIG-I has a tandem CARD, RNA helicase domain, and CTD. Positions of the mutations are indicated by *asterisks*. *aa*, amino acids. *B*, FLAG-tagged WT RIG-I and SNPs were produced in RIG-I$^{-/-}$ MEFs and detected by immunoblotting using an anti-FLAG antibody.

loss of function mutations of RIG-I and MDA5. Notably, two MDA5 mutations, E627* and I923V, recently reported to have a strong association with resistance to T1D (13), were severely inactive. The results suggest a novel molecular mechanism for the activation of RLRs and will contribute to our understanding of the functional effects of RLR polymorphisms and the critical relationship between RLR nsSNPs and diseases.

EXPERIMENTAL PROCEDURES

Cells, DNA Transfection, and Preparation of Cell Extracts—L929 cells were maintained in minimum essential medium Eagle (Sigma) with 5% fetal bovine serum and penicillin/streptomycin. Mouse embryonic fibroblasts (MEFs) were obtained from Dr. S. Akira (Osaka University). MEFs and 293T cells were maintained in Dulbecco's modified Eagle's medium with 10% fetal bovine serum and penicillin/streptomycin. L929 cells were transiently transfected with the DEAE-dextran method. MEFs and 293T cells were transiently transfected by FuGENE 6 (Roche Applied Science). For the preparation of cell extracts, cells were lysed with lysis buffer (50 mM Tris-HCl, pH 7.5, 150 mM NaCl, 1 mM EDTA, 1% Nonidet P-40, 0.1 mg/ml leupeptin, 1 mM phenylmethylsulfonyl fluoride, and 1 mM sodium orthovanadate) and centrifuged at 245,000 × *g* for 10 min. The supernatant was used for SDS-PAGE and electrophoretic mobility shift assays (EMSAs).

Oligonucleotides—Oligonucleotides (800 bp) corresponding to the coding sequence of green fluorescent protein were amplified by PCR using T7-primer (5′-CGTAATACGACTCACTATAGGGGATATCAGCAAAGGAGAAGAACTTTT-3′) and T3-primer (5′-GCAATTAACCCTCACTAAAGGGAGGCCTAGGGAGAAGACAGTGAGCTC-3′). Long dsRNA (ds800) was prepared by annealing complementary strands separately synthesized by *in vitro* transcription using the AmpliScribe T7 flash transcription kit (EPICENTRE Biotechnologies) and the AmpliScribe SP6 high yield transcription kit (EPICENTRE Biotechnologies). The annealed dsRNA was treated with S1 nuclease (Takara Bio) to generate a blunt end and alkaline phosphatase (Takara Bio) to remove 5′-phosphate. ^{32}P-ds800 was prepared by labeling the 800-bp dsRNA using T4 polynucleotide kinase and [γ-^{32}P]ATP.

Reporter Assay—MEFs were transfected with p55-C1Bluc, pRLtK, and expression plasmids for RIG-I mutants or MDA5 mutants. Cells were split into two aliquots, stimulated with RNA (5′-pppGG25) (6) or poly(I-C) transfection or Sendai virus (SeV) infection for 12 h, and harvested at 48 h after DNA transfection. L929 cells were transfected similar to MEFs but were stimulated by Newcastle disease virus infection. The infections were performed as described previously (14). The RNA transfection and poly(I-C) transfection were performed using Lipofectamine™ RNAiMAX

Downloaded from www.jbc.org at OSAKA UNIVERSITY, on March 22, 2010

(Invitrogen). The luciferase assay was performed with a Dual-Luciferase reporter assay system (Promega). Luciferase activity was normalized using *Renilla* luciferase activity (pRLtk) as a reference.

Quantitative PCR Assay—Quantitative PCR was performed as described previously (3).

Plasmid Constructs—p-55C1Bluc and pRLtk, pEF-FLAG-RIG-I, pEF-FLAG-RIG-ICARD, pEF-FLAG-MDA5, and pEF-FLAG-MDA5CARD were described previously (14). Data on SNPs for *RIG-I* and *MDA5* were obtained from the NCBI (www.ncbi.nlm.nih.gov) and HapMap databases. The expression plasmids for RIG-I mutants (pEF-FLAG-RIG-IR7C, pEF-FLAG-RIG-IS144F, pEF-FLAG-RIG-IS183I, pEF-FLAG-RIG-IT260P, pEF-FLAG-RIG-II406T, pEF-FLAG-RIG-ID580E, pEF-FLAG-RIG-IF789L, and pEF-FLAG-RIG-ICARDS183I) and MDA5 mutants (pEF-FLAG-MDA5T260S, pEF-FLAG-MDA5L274I, pEF-FLAG-MDA5K351E, pEF-FLAG-MDA5I442V, pEF-FLAG-MDA5H460R, pEF-FLAG-MDA5E627*, pEF-FLAG-MDA5H843R, pEF-FLAG-MDA5I923V, pEF-FLAG-MDA5A946T, and pEF-FLAG-MDA5D1014E) were generated using a GeneEditor *in vitro* site-directed mutagenesis system (Promega). The mutations were confirmed by sequencing.

Antibodies and Immunoblotting—The anti-FLAG (M2; Sigma) antibody is a commercial product. SDS-PAGE and immunoblotting were performed as described previously (14).

EMSA—293T cells (1×10^6/6-cm dish) were transfected with 1 μg of expression vector. At 24 h after transfection, cell extract was prepared and mixed with anti-FLAG beads (Sigma) to adsorb FLAG-tagged proteins. The beads were washed, and bound protein was eluted with FLAG peptide (Sigma). The method of EMSA was described previously (6).

RESULTS

Construction of RIG-I Mutants and Their Biological Activities in MEFs Derived from RIG-I Knock-out Mice—nsSNPs were selected from nucleotide sequence polymorphisms of human RIG-I reported in databases and introduced into the RIG-I expression vector by site-directed mutagenesis. Domain structure and locations of the mutations are indicated in Fig. 1*A*. In RIG-I$^{-/-}$ MEFs transiently transfected with these vectors, the wild type and seven human RIG-I mutants were expressed at comparable levels (Fig. 1*B*). These results indicate that none of the amino acid substitutions significantly affect the synthesis and/or stability of RIG-I. The signaling function of the mutants was analyzed by temporarily complementing the function of RIG-I in RIG-I$^{-/-}$ MEFs using a virus-responsive luciferase reporter gene (Fig. 2*A*). Although the transfection of 5′-pppRNA did not activate the reporter gene significantly in RIG-I$^{-/-}$ MEFs (Fig. 2*A*, *Vector*), the ectopic expression of WT RIG-I restored the responsiveness to the ligand. All the mutant constructs exhibited functional complementation except the R7C, S144F, and S183I mutants, which exhibited a reduced response to 5′-pppRNA, particularly the S183I mutant, which exhibited a severe defect. Because the activity of S144F was not reproducible, we did not investigate this mutant further. It has been shown that RIG-I senses SeV and activates the IFN promoter. Therefore, the ability of the mutants to respond to this viral inducer was tested (Fig. 2*B*). SeV efficiently activated the reporter

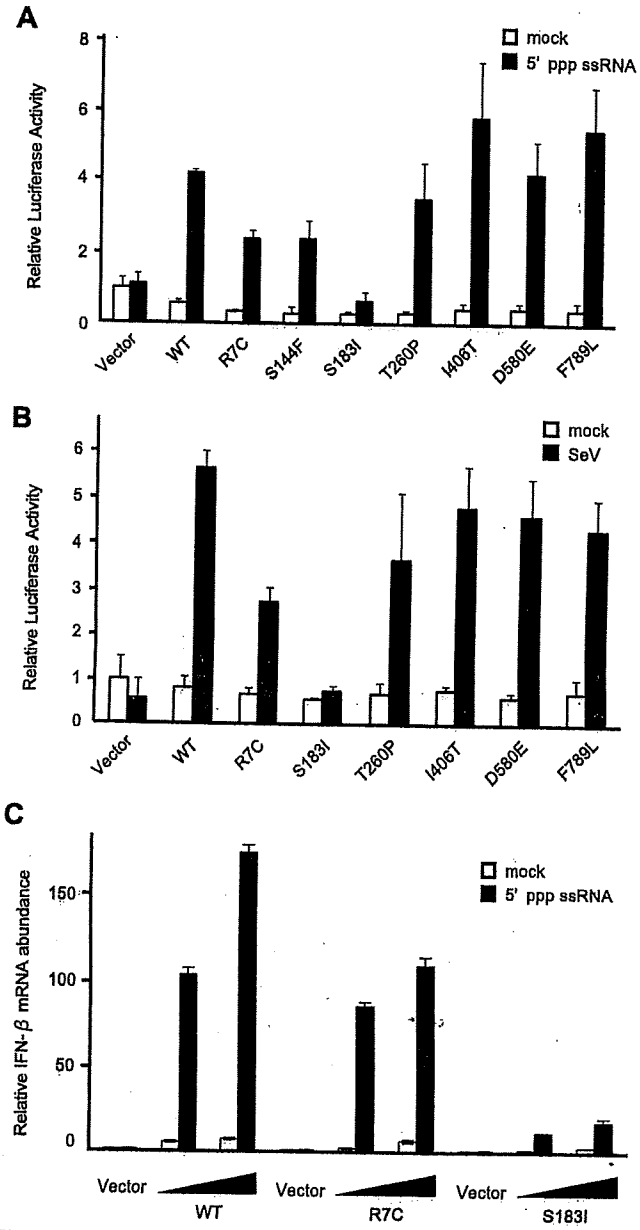

FIGURE 2. **Functional analysis of RIG-I nsSNP mutants.** *A* and *B*, RIG-I$^{-/-}$ MEF cells were transiently transfected with p-55CIBluc together with empty vector (*Vector*) or the indicated constructs. The cells were subjected to a Dual-Luciferase assay after stimulation with 5′-ppp-ssRNA (12 h) (*A*) or SeV (12 h) (*B*). The relative firefly luciferase activity, normalized to the *Renilla* luciferase activity, is shown. *Error bars* show the SDs for triplicate transfections. *mock*, mock-treated. *C*, RIG-I$^{-/-}$ MEFs were transfected with empty vector (*Vector*) or expression vectors for WT RIG-I or mutants as indicated (the total amount of plasmid was kept at 6 μg by adding empty vector). To observe the dose response, cells were transfected with 3 or 6 μg of the expression plasmid. Cells were mock-treated or transfected with 5′-ppp-ssRNA for 12 h, and *IFN-β* mRNA was quantified by quantitative PCR by using the Applied Biosystems primer set for mouse interferon-β1: Mm00439546_S1.

gene when WT RIG-I was expressed; however, S183I was virtually inactive and R7C exhibited partial activity. Other mutants sensed the virus as efficiently as the WT. We further confirmed the effect of the R7C and S183I mutations by monitoring the expression of endogenous mouse *IFN-β* mRNA (Fig. 2*C*). The results clearly demonstrate that S183I is barely active and that R7C is partially

Downloaded from www.jbc.org at OSAKA UNIVERSITY, on March 22, 2010

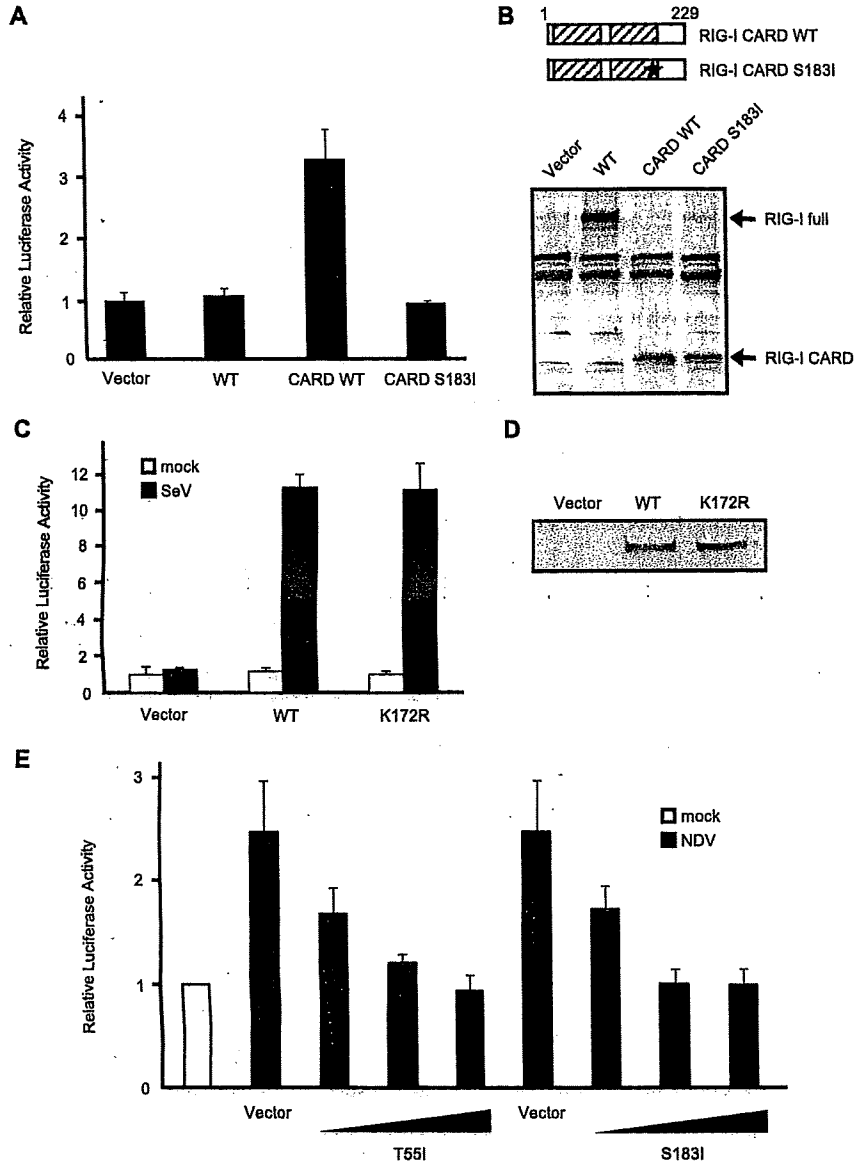

FIGURE 3. **Characterization of RIG-I S183I.** *A*, RIG-I$^{-/-}$ MEF cells were transfected with reporter genes together with empty vector (*Vector*) or plasmid expressing FLAG-tagged WT RIG-I, RIG-I CARD (the N-terminal region, amino acid 1–229), or RIG-I CARD S183I. After transfection (24 h), the cells were subjected to a Dual-Luciferase assay. *Error bars* show the S.D. values for triplicate transfections. *B*, each protein expressed in RIG-I$^{-/-}$ MEF cells was detected by immunoblotting using an anti-FLAG antibody. *RIG-I full*, full-length RIG-I. *C*, reporter assay of the K172R mutant was performed as in Fig. 2*B*. *D*, protein levels were determined by immunoblotting. RIG-I K172R and WT RIG-I were expressed at comparable levels. *E*, empty vector or expression vectors for full-length RIG-I with the T55I or S183I mutation were introduced into L929 cells (the total amount of plasmid was kept at 9 μg by adding empty vector) and infected with Newcastle disease virus, and reporter activity was analyzed as in *panel A*. To observe the dose response, cells received 1, 5, or 9 μg of the expression plasmid for T55I and S183I as indicated. *NDV*, Newcastle disease virus.

active. The above results strongly suggest that Ser-183 is critical for RIG-I to sense transfected 5′-pppRNA as well as SeV-derived PAMPs. Ser-183 resides within the second CARD, and this prompted us to explore the impact of the S183I substitution on the signaling function of the isolated RIG-I CARD. Unlike that of the full-length RIG-I, overexpression of the truncated RIG-I (1–229), which encompasses the two repeats of CARD, constitutively activated the reporter p-55C1B without a viral stimulus (Fig. 3*A*). However, RIG-I (1–229) with S183I failed to activate the reporter gene. In these cells, levels of RIG-I (1–229) with or without the S183I mutation were comparable, suggesting that Ser-183 is critical for the signaling function but does not affect protein levels of RIG-I CARD (Fig. 3*B*). It was reported that human RIG-I undergoes ubiquitination at Lys-172 in the second CARD, and this process is essential for RIG-I signaling (15). To compare the mutation at Ser-183, we generated a K172R mutant and tested its activity (Fig. 3, *C* and *D*). Surprisingly, the mutant exhibited virus-induced signaling activity comparable with the WT, suggesting that the ubiquitination of Lys-172 plays a minor role in the regulation of RIG-I and that the phenotype of the S183I mutant is unlikely due to a failure of ubiquitination.

It is known that human RIG-I with the amino acid substitution T55I acts as a dominant inhibitor (7). This mutation within the first CARD inactivates the signaling function of the isolated tandem CARDs. We next tested whether RIG-I S183I exhibits a dominant negative phenotype. L929 cells were transfected with control vector or RIG-I mutants and then activated by infection of Newcastle disease virus. Cells transfected with the vector exhibited *IFN* promoter activity due to endogenous RIG-I (Fig. 3*E*). Expression of T55I as well as S183I significantly reduced the promoter activity in a dose-dependent manner, suggesting that S183I causes a dominant negative phenotype similar to T55I.

Construction of MDA5 Mutants and Their Biological Activities in MEFs Derived from MDA5 Knockout Mouse—Next, the biological activity of human MDA5 mutants was analyzed similarly using *MDA5*-deficient MEFs. Ten nsSNPs including A946T identified in familial T1D (16) were introduced into the MDA5 expression vector (Fig. 4*A*). The wild type and mutants were expressed in MDA5$^{-/-}$ MEFs at comparable levels (Fig. 4*B*), showing that the mutations, including the E627* truncation, did not affect MDA5 protein levels. The biological activity of the mutants was assayed similarly to that of the RIG-I mutants. As a MDA5 agonist, a commercial poly(I-C) with an average length of 2 kbp was used, which selectively activates MDA5 (6, 11). Wild-type MDA5 clearly conferred responsiveness to the poly(I-C) (Fig. 5). Eight MDA5 mutants, including A946T, which was implicated in human T1D (16), exhibited complementing activity comparable

Downloaded from www.jbc.org at OSAKA UNIVERSITY, on March 22, 2010